

EVALUATION AND OPTIMIZATION OF PERVIOUS CONCRETE
WITH RESPECT TO PERMEABILITY AND CLOGGING

A Thesis

by

YOUNG MIN JOUNG

Submitted to the Office of Graduate Studies of
Texas A&M University
in partial fulfillment of the requirements for the degree of

MASTER OF SCIENCE

December 2008

Major Subject: Civil Engineering

EVALUATION AND OPTIMIZATION OF PERVIOUS CONCRETE
WITH RESPECT TO PERMEABILITY AND CLOGGING

A Thesis

by

YOUNG MIN JOUNG

Submitted to the Office of Graduate Studies of
Texas A&M University
in partial fulfillment of the requirements for the degree of

MASTER OF SCIENCE

Approved by:

Chair of Committee, Zachary C. Grasley
Committee Members, A. K. Mukhopadyay
Charles W. Graham
Head of Department, David V. Rosowsky

December 2008

Major Subject: Civil Engineering

ABSTRACT

Evaluation and Optimization of Pervious Concrete with Respect to
Permeability and Clogging.

(December 2008)

Young Min Joung, B.S., University of Incheon

Chair of Advisory Committee: Dr. Zachary C. Grasley

Although pervious concrete was first used in the nineteenth century, it has only recently begun to increase in popularity. As urban areas expand, the problems associated with runoff management have become more challenging. The focus on the negative environmental effects associated with pavement runoff has also increased. These two issues have spurred the recent interest in pervious concrete pavements. Pervious concrete, however, has deficiencies which limit its application as pavements. These limitations include low compressive strength, flexural strength, clogging, and other durability issues. The overall purpose of this project was to provide tools to evaluate and improve the durability and strength of pervious concrete such that it may be more confidently employed in urban roadways. The specific objectives of this project were to

- (a) investigate the effect of mixture design on strength of pervious concrete (including the effect of fibers),
- (b) evaluate effect of clogging materials on coefficient of permeability,
- (c) and investigate the use of the dynamic pressurization test to evaluate the durability of pervious concrete,

(d) develop a simple model for predicting removal of clogging particles from pervious concrete pavement surface pores.

This thesis documents the results of the laboratory testing, and presents recommendations for mixture proportioning. In addition, recommendations are provided for optimizing the balance between compressive strength and permeability.

To My Parents, Taeyoung Joung, Soonbok Ko

ACKNOWLEDGEMENTS

Special thanks to Dr. Grasley for his guidance and advice in this research and also for giving me an opportunity to participate in this project. I could not have accomplished all this without Dr. Grasley's assistance. My appreciation goes to my committee members, Dr. Mukhopadyay and Dr. Graham, for their guidance and support throughout the course of this research. I am grateful to Cris who reviewed this paper and gave me advice.

TABLE OF CONTENTS

| | Page |
|---|------|
| ABSTRACT | iii |
| DEDICATION | v |
| ACKNOWLEDGEMENTS | vi |
| TABLE OF CONTENTS | vii |
| LIST OF FIGURES..... | x |
| LIST OF TABLES | xi |
| 1 INTRODUCTION..... | 1 |
| 1.1 Problem Statement | 1 |
| 1.2 Research Objective..... | 2 |
| 1.3 Research Scope | 3 |
| 2 LITERATURE REVIEW..... | 4 |
| 2.1 History of Pervious Concrete | 4 |
| 2.2 Advantages of Pervious Concrete | 6 |
| 2.3 Common Applications..... | 7 |
| 2.4 Durability | 7 |
| 2.5 Compressive Strength | 9 |
| 2.6 Flexural Strength..... | 21 |
| 2.7 Permeability | 23 |
| 2.8 Clogging..... | 25 |
| 2.9 Mixture Proportion..... | 28 |
| 2.10 Pervious Concrete Pavement Design and Maintenance..... | 29 |

| | Page |
|--|------|
| 3 MATERIALS INVESTIGATION | 33 |
| 3.1 Aggregate Properties | 33 |
| 3.2 Mixture Proportions | 35 |
| 3.3 Specimen Preparation..... | 37 |
| 4 EFFECT TO MIXTURE DESIGN ON STRENGTH OF PERVIOUS CONCRETE | 39 |
| 4.1 Testing Procedures | 39 |
| 4.2 Results | 40 |
| 5 EFFECT OF MIXTURE DESIGN ON PERMEABILITY AND CLOGGING OF PERVIOUS CONCRETE | 54 |
| 5.1 Permeability Measurement..... | 54 |
| 5.2 Clogging Test | 56 |
| 5.3 Results | 58 |
| 6 EVALUATION OF DYNAMIC PRESSURIZATION TEST TO EVALUATION DURABILITY OF PERVIOUS CONCRETE | 64 |
| 6.1 Motivation | 64 |
| 6.2 DP Test Theory and Introduction..... | 65 |
| 6.3 Application of DP Test to Pervious Concrete | 67 |
| 6.4 Experimental Apparatus and Procedure | 72 |
| 6.5 Initial Trials and Results | 75 |
| 7 SUCTION MODEL | 81 |
| 7.1 Motivation | 81 |
| 7.2 Suction Model Introduction and Assumption | 82 |
| 7.3 Suction Model Assumptions and Derived Equations for Y_{particle} | 84 |
| 7.4 Evaluation of Maximum Distance, X_{max} | 91 |
| 7.5 Evaluation of the Vertical Position of Particle..... | 96 |

| | Page |
|--|------|
| 8 SUMMARY | 101 |
| 9 RECOMMENDATION AND CONCLUSIONS..... | 106 |
| 9.1 Recommendation on Mixture Proportioning..... | 106 |
| 9.2 Conclusions | 107 |
| REFERENCES..... | 109 |
| VITA | 117 |

LIST OF TABLES

| | | Page |
|---------|---|------|
| Table 1 | Relationship between void ratio and seven-day compressive strength, after Schaefer et al.(2006)..... | 11 |
| Table 2 | Relationship between 28-day compressive strength and unit weight, after Meininger (1988) | 12 |
| Table 3 | Properties of aggregate used in the pervious concrete mixes..... | 33 |
| Table 4 | Pervious concrete mixtures investigated in this study | 36 |
| Table 5 | Paste layer thickness and mixture design parameters necessary for the calculation of the thickness..... | 72 |
| Table 6 | Input values for equation (45)..... | 95 |

LIST OF FIGURES

| | Page |
|---|------|
| Figure 1 Relationship between void ratio and seven-day compressive strength, after Schaefer et al.(2006)..... | 11 |
| Figure 2 Relationship between 28-day compressive strength and unit weight, after Meininger (1988) | 12 |
| Figure 3 Relationship between seven-day compressive strength and unit weight, after Zouaghi et al. (2000)..... | 13 |
| Figure 4 Relationship between compressive strength and w/c, after Meininger (1988)..... | 15 |
| Figure 5 Relationship between w/c and compressive strength (cement content = 239 kg/m ³), after Meininger (1988)..... | 16 |
| Figure 6 Relationship between compressive strength and cement content, after Zouaghi et al. (2000)..... | 17 |
| Figure 7 Relationship between sand content and compressive strength of pervious concrete, after Meininger..... | 18 |
| Figure 8 Effect of silica fume addition on the seven-day compressive strength, after Schaefer et l.(2006) | 19 |
| Figure 9 Effect of coarse aggregate size on compressive strength of pervious concrete, after Schaefer et al. (2006)..... | 20 |
| Figure10 Relationship between flexural strength and total porosity, after Marolf et al. (2004)..... | 21 |
| Figure 11 Relationship between flexural strength and characteristic pore size, after Marolf et al. (2004)..... | 22 |
| Figure 12 Comparison of the effect of void ratio on compressive and flexural strength using data from Meininger (1988). | 23 |

| | Page |
|---|------|
| Figure 13 Relationship between pervious concrete void ratio and permeability for mixes placed using regular compaction energy, after Schaefer et al. (2006)..... | 24 |
| Figure 14 Gradation of type A ,B, and C after Othman and Hardiman (2005); Fwa et al. (1999)..... | 26 |
| Figure 15 Relationship between mass of clogging soil and permeability in asphalt porous friction course pavement material using data from Fwa, et al. (1999)..... | 28 |
| Figure 16 Comparison of typical range of aggregate proportions in pervious concrete mixtures versus approximate ACI normal concrete mixtures. | 29 |
| Figure 17 Typical cross-section of pervious concrete pavement, after Tennis et al. (2004)..... | 30 |
| Figure 18 Typical parking & driveway pervious concrete pavement, after (www.stonecreekmaterials.com). | 31 |
| Figure 19 Pervious concrete pavement design for heavy traffic, after (www.stonecreekmaterials.com). | 32 |
| Figure 20 Pervious concrete pavement design for sidewalk, cart path, hike, and bike trails, after (www.stonecreekmaterials.com). | 32 |
| Figure 21 Gradation of sand used in this study..... | 34 |
| Figure 22 6 in. x 12 in. cylindrical sample and 6 in. x 6 in. x 18 in. beam sample..... | 38 |
| Figure 23 Picture of samples (from left to right, low coarse aggregate, mid coarse aggregate, and high coarse aggregate)..... | 41 |

| | Page |
|---|------|
| Figure 24 Higher paste content (left) and lower paste content (right). As volume of coarse aggregate increases, volume of paste decrease. | 41 |
| Figure 25 Effect of coarse aggregate content on compressive strength evolution (high coarse agg = high volume of coarse aggregate, mid coarse agg = middle amount of coarse aggregate, low coarse agg = low volume of coarse aggregate). | 42 |
| Figure 26 The top of sample incorporating both 9.5 mm and 12.5 mm aggregates. The white circle indicates a region of poor compaction. | 44 |
| Figure 27 The side of sample incorporating both 9.5 mm and 12.5 mm aggregates. The white circles indicate regions of poor compaction. | 44 |
| Figure 28 Effect of aggregate size on compressive strength. | 45 |
| Figure 29 Effect of cementitious materials on compressive strength. | 45 |
| Figure 30 Relationship between void ratio and 28-day compressive strength. The numbers in the Figure denote different mixtures as shown in Table 4. | 47 |
| Figure 31 Relationship between void ratio and flexural strength. | 49 |
| Figure 32 6 in. x 6 in. x 12 in. beam sample after flexural test (polypropylene). | 50 |
| Figure 33 Illustration of why addition of fibers does not significantly increase flexural strength. Since bonding is poor, fibers are not strongly bonded to paste so that even low stress leads fibers to pull out. | 50 |

| | Page |
|--|------|
| Figure 34 Comparison of the inter-aggregate gap in mixtures using 12.5 mm aggregate (A) or a combination of 9.5 mm and 12.5 mm (B). The large space between aggregates in (A) leads pervious concrete beam to easily fail in tension. | 51 |
| Figure 35 Relationship between 14-day compressive strength and unit weight. | 52 |
| Figure 36 Relationship between 28-day compressive strength and unit weight. | 53 |
| Figure 37 Relationship between flexural strength and unit weight. | 53 |
| Figure 38 Falling-head permeameter used to measure coefficient of permeability of pervious concrete. | 55 |
| Figure 39 Device used to clog pervious concrete cylinders using sand/water mixture. | 57 |
| Figure 40 Clogged sample after clogging test. Sand is present in pores, and excessive sand is apparent on the surface of the sample. | 57 |
| Figure 41 Relationship between void ratio and coefficient of permeability for all mixtures. | 59 |
| Figure 42 Relationship between coefficient of permeability and 28 day compressive strength. | 60 |
| Figure 43 Relationship between amount of clogging material added to the specimens and coefficient of permeability. High coarse agg (12.5 mm) = high volume of coarse aggregate, mid coarse agg (12.5 mm) = middle volume of coarse aggregate, low coarse agg (12.5 mm)= low volume of coarse aggregate. | 62 |
| Figure 44 Sand flushed from sample after clogging test. Marked circles show sand that was flushed out during the permeability test. | 63 |

| | Page |
|---|------|
| Figure 45 Illustration how pervious concrete is considered as a sphere model for the DP test..... | 67 |
| Figure 46 Comparison of cylinder and sphere relaxation functions, after Scherer (2006)..... | 69 |
| Figure 47 Illustration of an aggregate covered with cement paste. (r_a = radius of aggregate, r_b = radius of aggregate + paste, R = layer thickness of paste). | 70 |
| Figure 48 Apparatus for dynamic pressurization experiment, after Grasley (2006)..... | 74 |
| Figure 49 Illustration of dynamic pressurization experiment. The sample is placed in the vessel. The pressure in the vessel (P_V), the pore fluid (P_p), and atmospheric pressure (P_0) are equal. After starting the test ($t=0^+$), P_V increases up to some higher value (P_A). Simultaneously, the sample contracts by the changed pressure. The fluid gradually flows through the sample such that the pore pressure eventually reaches P_A . At long times, the final strain (ϵ_∞) is constant as the pore fluid pressure reaches P_A , after Scherer (2006)..... | 74 |
| Figure 50 Typical long term response of pervious concrete to dynamic pressurization. Paste layer is influenced first, followed by pressurization of the aggregates. Entrapped air may affect inflection of point A. | 77 |
| Figure 51 $\Omega(t)$ versus t on mixture A..... | 78 |
| Figure 52 $\Omega(t)$ versus t on mixture B..... | 79 |
| Figure 53 $\Omega(t)$ versus t on mixture C..... | 80 |
| Figure 54 Illustration of clogged pore in pervious concrete pavement while the vehicle wheel is passing over. | 82 |

| | Page |
|---|------|
| Figure 55 Illustration of upward and downward force, which influence position of particle in pore structure. | 84 |
| Figure 56 Geometry between tire and pore in pavement surface is described. | 86 |
| Figure 57 Geometry explaining how volume of water in pore structure is changed when vehicle tire passes over. | 88 |
| Figure 58 radius of pore structure vs P_{max} | 93 |
| Figure 59 Relationship between horizontal distance and vertical position of particle in terms of various vehicle speed. | 97 |
| Figure 60 Relationship between horizontal distance and vertical position of particle in terms of various density of clogging materials. | 98 |
| Figure 61 Relationship between horizontal distance and vertical position of particle in terms of various radius size of pore in pervious concrete. | 99 |
| Figure 62 Relationship between distance and vertical position of particle in terms of Y_{sink} and Y_{fluid} | 100 |

1 INTRODUCTION

1.1 Problem Statement

Since the U.S. Environmental Protection Agency (EPA) has increased regulations for stormwater management, there has been a need for pavements that minimize surface runoff. Often, traditional construction of roadways is unable to effectively manage stormwater runoff.

Pervious concrete is a potential solution for eliminating at least some stormwater runoff. The high level of interconnected macroporosity in pervious concrete effectively minimizes runoff from paved areas. In addition, pervious concrete has other advantages. For instance, pervious concrete is quieter to drive on than ordinary pavement since the porous pavement absorbs sound (Olek et al., 2003). Pervious concrete can remove stormwater more quickly than traditional concrete (Schaefer et al., 2006) which results in improved skid resistance.

However, pervious concrete has several limitations preventing widespread application to normal roadways. The limitations of pervious concrete are linked to strength, durability, and maintenance.

Pervious concrete has low compressive and flexural strength compared to ordinary concrete. This drawback is one of the limitations that prevent pervious concrete from

being confidently employed for pavements. Since pervious concrete contains a minimum of fine aggregate, strength depends primarily on the interaction between cement paste and coarse aggregate. The high porosity in pervious concrete reduces compressive and flexural strength. Concrete for pavement applications typically has compressive strength ranging from 3,000 to 4,000 psi (Kosmatka et al., 2002). On the other hand, conventional compressive strength of pervious concrete is in the range from 800 to 3,000 psi (Tennis et al., 2004).

Durability of pervious concrete must be considered for long-term performance. In general, durability of pervious concrete is dependent on degree of saturation and exposure to freezing-thawing conditions (Yang et al., 2006). Very few research projects have investigated the durability of pervious concrete.

Clogging of the concrete material is an additional problem for pervious concrete. Debris and dirt fill the pore network such that pervious concrete does not drain properly.

Clogging affects not only permeability, but also durability. Both debris and dirt accumulated over some period of time reduce permeability (Rogge, 2002). Moreover, the durability of pervious concrete is reduced when clogging maintains a high level of saturation within the concrete (Yang et al., 2006).

1.2 Research Objective

The purpose of this project is to provide tools to evaluate and improve the durability and strength of pervious concrete such that it may be more confidently employed in urban

roadways, driveways, and parking lots. An additional project is to develop a useful tool for predicting removal of clogging particles from pervious concrete pavement surface pores through suction induced by vehicle tires passing over the clogged pore.

1.3 Research Scope

Pervious concrete mixtures prepared in this research used a bimodal coarse aggregate gradation. The mixtures contained two different single-sized coarse aggregates such as 12.5 mm (1/2 in.), and 9.5 mm (3/8 in.). All mixtures included a small amount of sand in accordance with typical pervious concrete mixtures found in the literature.

The concrete mixtures were investigated to evaluate the characteristics of pervious concrete, including the time development of strength, permeability, and clogging potential. In addition, a new technique was evaluated for measuring the intrinsic permeability of the cement paste layers binding the aggregates together in the pervious concrete as a means to assess the durability of pervious concrete.

2 LITERATURE REVIEW

2.1 History of Pervious Concrete

Pervious concrete is also referred to as no-fine aggregate concrete or gap-graded concrete. Pervious concrete has been employed in European countries since the nineteenth century (Francis, 1965). Europeans have used pervious concrete in various ways, including cast in place load bearing walls, prefabricated panels, and steam cured blocks.

The earliest usage of pervious concrete in modern history was for two houses in England. Over 900 houses were built by 1942. Most houses using pervious concrete are in the United Kingdom (ACI 522 Pervious Concrete, 2006).

After World War II, the application of pervious concrete spread all over the world to Europe, Africa, Venezuela, the Middle East, and Australia. Pervious concrete generally does not require as much cement paste compared with traditional concrete, motivating its increased usage. Despite the advantages of the pervious concrete, the number of buildings and houses utilizing pervious concrete in North America was fairly restricted (ACI 522 Pervious Concrete, 2006) because of the material limitations listed in Section 1.1.

Recently, pervious concrete usage in the U.S. has begun to increase. In particular, certain states such as Florida, Utah, and New Mexico have been required to reduce uncontrolled stormwater runoff. California, Illinois, Oklahoma, and Wisconsin have applied pervious concrete for permeable base and edge drains (Mathis, 1990). The use of pervious concrete meets the needs of Best Management Practice (BMP) of the Environmental Protection Agency (EPA), which will lead to additional growth in pervious concrete application.

Traditional pervious concrete has not been typically employed for highways and local roadways. Although pervious concrete is versatile, the limitations of pervious concrete have hindered the design for typical traffic loads, soil with low permeability, heavy vehicular traffic, and resurfacing with impermeable materials (U.S. EPA, 1999).

Pervious concrete has been passively used as a drainable base, or sub-base material. In addition, pervious concrete has been implemented for a roadway surface or friction-coarse (ACI 522 Pervious Concrete, 2006), primarily for the low noise release and high water absorption (Sandberg and Ejsmont 2002; Beeldens et al., 2004; Nakahara et al., 2004) of such a surface layer. Since a thin surface layer of pervious concrete has better resistance to rutting than porous asphalt, pervious concrete has been utilized in place of porous asphalt surface courses in Japan to improve safety and ride quality (Nakahara et al., 2004).

2.2 Advantages of Pervious Concrete

2.2.1 Noise

Pervious concrete has the ability to decrease the noise emitted by vehicles on concrete pavements due to reduction of interaction noise between the tire and pavement. Porous pavement absorbs the sound (Olek et al., 2003). To be specific, the characteristics of pervious concrete minimize air pumping between the tire and road surface (ACI 522 Pervious Concrete, 2006). Therefore, pervious concrete has the potential to diminish greatly the noise generated by vehicles (Sandberg and Ejsmont, 2002). Constructing fences in urban areas to block road noise could prove costly. Instead, constructing pervious concrete on the road should reduce noise as well as the expense (Nelson and Philips, 1994; Descornet, 2000). The thickness of the pervious concrete pavement layer is closely related to the noise reduction (Beeldens et al., 2004).

2.2.2 Skid Resistance

Pervious concrete can remove storm water more rapidly than traditional concrete (Schaefer et al., 2006) due to its higher absorption capacity and more rapid infiltration of stormwater into the ground. By minimizing water on the pavement surface, skid resistance is dramatically improved.

2.2.3 Stormwater Runoff

Reducing stormwater runoff is one of the primary functions of pervious concrete.

Pervious concrete contains minimal fine aggregate and contains uniformly sized coarse aggregate so that more void space exists in the matrix for holding and transporting water

(Zouachi et al, 2000). Pervious concrete can substantially reduce surface runoff water in comparison to traditional concrete pavement. Thus, pervious concrete can reduce the size of necessary storm sewers (ACI 522 Pervious Concrete, 2006).

2.2.4 Native Ecosystem

Pervious concrete can filter pollutants in storm water runoff that would penetrate into the ground. As pervious concrete absorbs runoff water, it conserves this natural resource (NRMCA, 2004). Pervious concrete helps to direct would-be runoff into the soil for use by plants and for ground water recharge. This helps to conserve this precious natural resource.

2.3 Common Applications

Common applications using pervious concrete are following : Parking lots, patios, swimming pool decks, shoulders, greenhouses, zoo areas, noise barriers, building walls, sub-base for conventional concrete pavements, artificial reefs, sidewalks, pathways, walls, hydraulic structures, pavement edge drains, slop stabilization, low-volume pavements, low-water crossings, residential roads, alleys, driveways, sewage treatment plant sludge beds, beach structures, seawalls, bridge embankments, rigid drainage layers under exterior mall areas, solar energy storage systems, wall lining for drilled water wells (Schaefer et al., 2006; ACI 522 pervious concrete, 2006; Tennis, 2004).

2.4 Durability

Durability of concrete is substantially affected by the material permeability. Since pervious concrete facilitates mobility of moisture, one would expect this to affect

durability. The durability problems should not be analogous to traditional concrete since the permeability of pervious concrete is not same as traditional concrete; that is, traditional flow-through permeability is not a measure of durability for pervious concrete.

2.4.1 Freezing and Thawing

Pervious concrete can allow more moisture to freely transfer into the matrix so that pervious concrete has different durability problems compared to conventional concrete. Many researchers have investigated the durability problems of pervious concrete from various perspectives. Tennis mentioned three conditions that cause freeze/thaw durability problems in pervious concrete: First, if pervious concrete is clogged, it influences the movement of water in pervious concrete. Second, if the average daily temperature is below freezing for a long term in specific regions. Third, if the ground water table reaches within three feet of the top of the concrete, pervious concrete can become saturated (Tennis et al., 2004). Freezing and thawing damage happens quickly if large voids of pervious concrete become saturated (Neithalath et al., 2003).

Zaldo (2006) pointed out that pervious concrete durability problems are related to three primary factors: mix design, placement, and proper maintenance. Zaldo mentioned that freezing and thawing damage of pervious concrete depends on the level of saturation. Therefore, annual cleaning in severe conditions should be conducted in order to avoid freezing and thawing damage. The key of freezing and thawing problem is how freely water is allowed to flow through pervious concrete. Consequently, maintaining a clean

infiltration system should reduce the severity of freezing and thawing problems (Zaldo, 2006).

During freeze/thaw cycles, debonding takes place between the aggregates and the cement paste (Yang et al., 2006). Mixture materials containing sand and/or latex are more durable for freezing and thawing. Finally, compaction energy (which controls the macro pore structure) greatly influences the freeze-thaw durability of pervious concrete (Schaefer et al., 2006). The degree of saturation of the paste layers coating the coarse aggregate particles also affects the durability pervious concrete (Yang et al., 2006).

2.5 Compressive Strength

Though pervious concrete can be used for various applications, its primary drawback is low compressive strength. Since the paste layer between aggregates is thin, it can not provide sufficient compressive strength compared with traditional concrete. Thus, the usage of pervious concrete was limited in high volume pavements. Instead, pervious concrete was applied in parking lots, which do not require high compressive strength.

To broaden the application of pervious concrete through increased compressive strength, several factors should be considered such as the strength of paste, thickness of paste coating the aggregates, and the interface between aggregate and paste.

Using smaller coarse aggregate and mineral admixture is suggested as a suitable means to obtain higher strength with pervious concrete (Schaefer et al., 2006).

To be specific, the compressive strength of pervious concrete is related to several factors such as void ratio, unit weight, water-cement ratio, supplementary cementing materials, aggregate size, and aggregate to cement ratio.

2.5.1 Void Ratio

The data in Figure 1 includes various coarse aggregates such as river gravel, pea gravel, and limestone. This graph shows a general relationship between void ratio and seven-day compressive strength. Seven-day compressive strength of pervious concrete declines linearly as void ratio increases. For pervious concrete, the void ratio refers explicitly to the entrapped macro porosity and does not include entrained air, gel or capillary porosity.

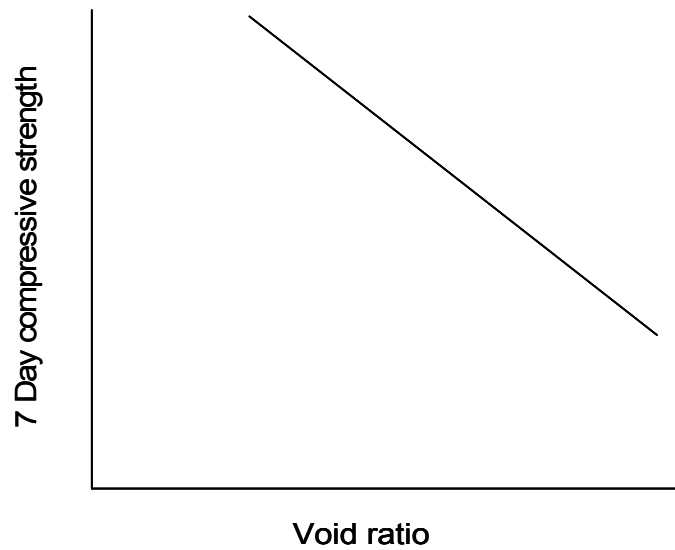


Figure 1 Relationship between void ratio and seven-day compressive strength, after Schaefer et al. (2006).

2.5.2 Unit Weight

Meininger (1988) investigated the relationship between 28-day compressive strength and unit weight. The relationship between compressive strength and unit weight is shown in Table 1 and Figure 2.

Table 1 Relationship between 28-day compressive strength and unit weight, after Malhotra (1976).

| w/c (by weight) | Unit weight (lbs/ft ³) | Compressive strength (psi) | w/c (by weight) | Unit weight (lbs/ft ³) | Compressive strength (psi) |
|--------------------|---------------------------------------|----------------------------------|--------------------|---------------------------------------|----------------------------------|
| 0.34 | 111 | 1355 | 0.31 | 107.5 | 975 |
| 0.34 | 110.5 | 1340 | 0.31 | 107.5 | 1050 |
| 0.34 | 112.5 | 1360 | 0.31 | 110 | 1100 |
| 0.34 | 114 | 1550 | 0.31 | 112 | 1395 |
| 0.34 | 120.8 | 1945 | 0.31 | 118 | 1540 |
| 0.34 | 122 | 2475 | 0.31 | 120.5 | 2095 |

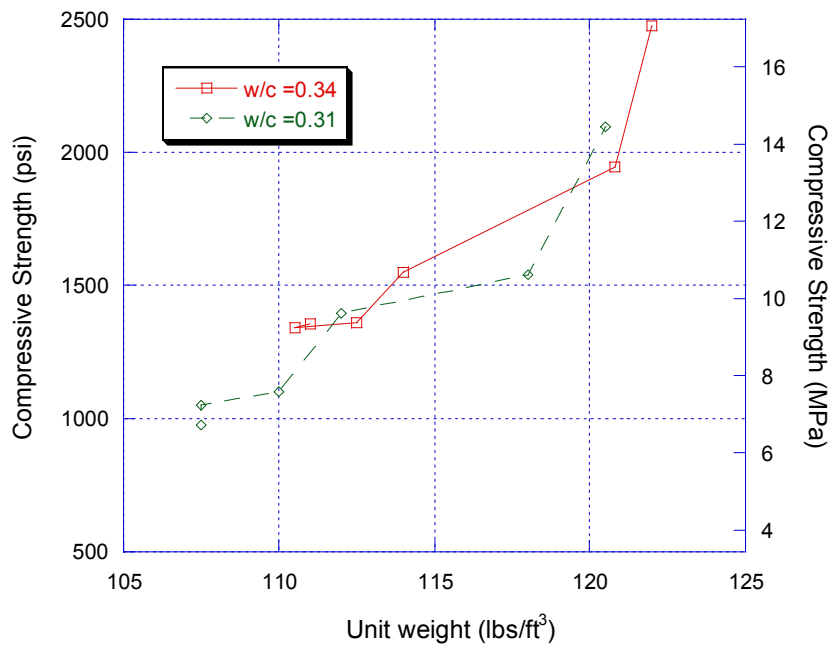


Figure 2 Relationship between 28-day compressive strength and unit weight, after Meininger (1988).

Zouaghi et al. (2000) introduced the relationship between compressive strength and unit weight shown in Figure 3. The mixtures were batched with water-cement ratio of 0.25. Since the unit weight of pervious concrete is directly linked to the percentage of voids in the material, it is not surprising that the compressive strength is linearly proportional to unit weight while inversely proportional to void ratio.

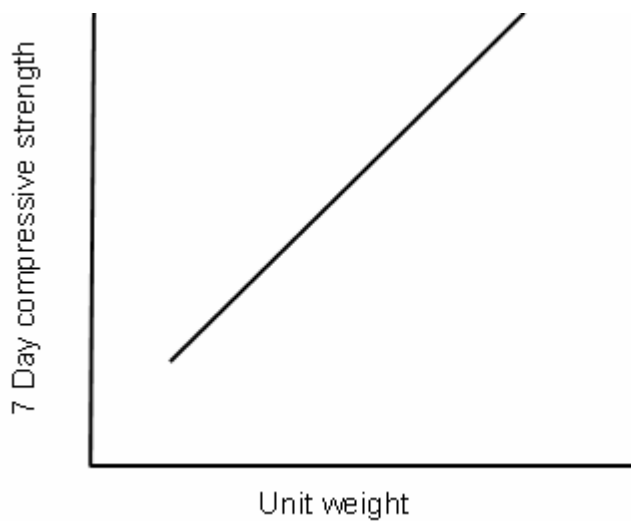


Figure 3 Relationship between seven-day compressive strength and unit weight, after Zouaghi et al. (2000).

2.5.3 Water/Cement Ratio

Meininger (1988) found that an intermediate water-cement ratio yielded the highest compressive strength, as shown in Table 2 and Figure 4. Both high and low water cement ratio had lower compressive strength than the intermediate level. Meininger suggested that this seemingly counter-intuitive result was due to poor cohesion between

the paste and aggregates at lower w/c. However, it should also be noted that at the lower w/c mixtures shown in Table 2, there is a lower paste content and a higher void content.

Table 2 Relationship between 28-day compressive strength and water cement ratio. (3/8" coarse aggregate, aggregate /cement ratio=6), after Meininger (1988).

| w/c | Cement (lb/yd ³) | Water (lb/yd ³) | Coarse aggregate (lb/yd ³) | Void content (%) | Strength (psi) | Percolation (in./min) |
|------|---------------------------------|--------------------------------|--|---------------------|-------------------|--------------------------|
| 0.51 | 440 | 224 | 2640 | 22 | 1350 | 5 |
| 0.47 | 430 | 203 | 2575 | 23 | 1370 | 4 |
| 0.43 | 430 | 184 | 2570 | 25 | 1500 | 10 |
| 0.39 | 425 | 165 | 2550 | 27 | 1400 | 30 |
| 0.35 | 415 | 145 | 2520 | 29 | 1250 | 40 |
| 0.31 | 410 | 125 | 2430 | 32 | 1010 | 51 |
| 0.27 | 395 | 106 | 2370 | 33 | 870 | 59 |

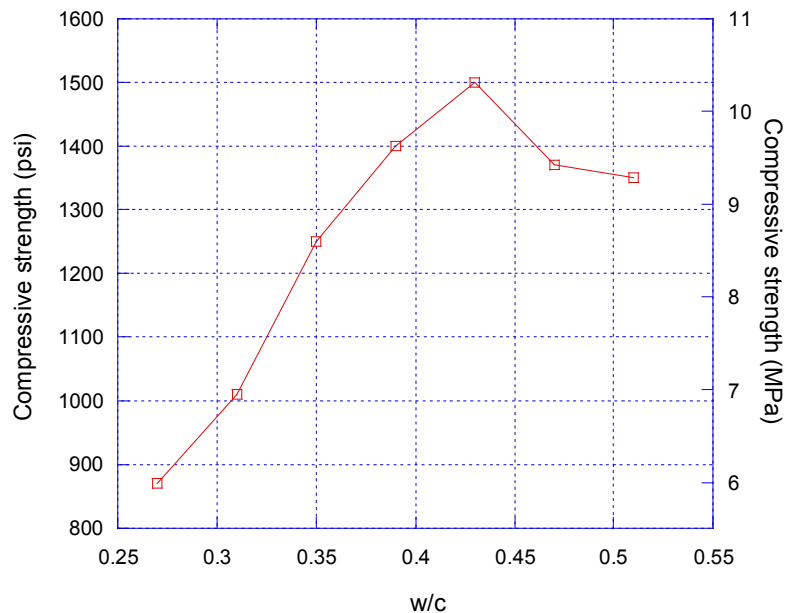


Figure 4 Relationship between compressive strength and w/c, after Meininger (1988).

Figure 5 shows the relationship between compressive strength as a function of water-cement ratio. The water-cement ratio which yields the highest compressive strength ranges from 0.3 to 0.35 if cement paste content is held constant. When water-cement ratio is low, it does not show high compressive strength due to poor workability and poor hydration of the cement, and poor cohesion of the cement paste to the aggregates.

Since hydration of cement needs the proper amount of water, reducing this amount of water reduces the hydration of cement. On the other hand, high water content shows low compressive strength through the formation of additional capillary porosity and the resulting reduction in the tensile capacity of the paste layers bonding the aggregates together. Though workability is good, high amounts of water reduce strength. Hence,

Figure 5 shows that the range from 0.3 to 0.35 is the optimum water-cement ratio for pervious concrete with respect to compressive strength. However, an important realization is that for pervious concrete, paste content and void ratio tend to be more influential on strength than w/c.

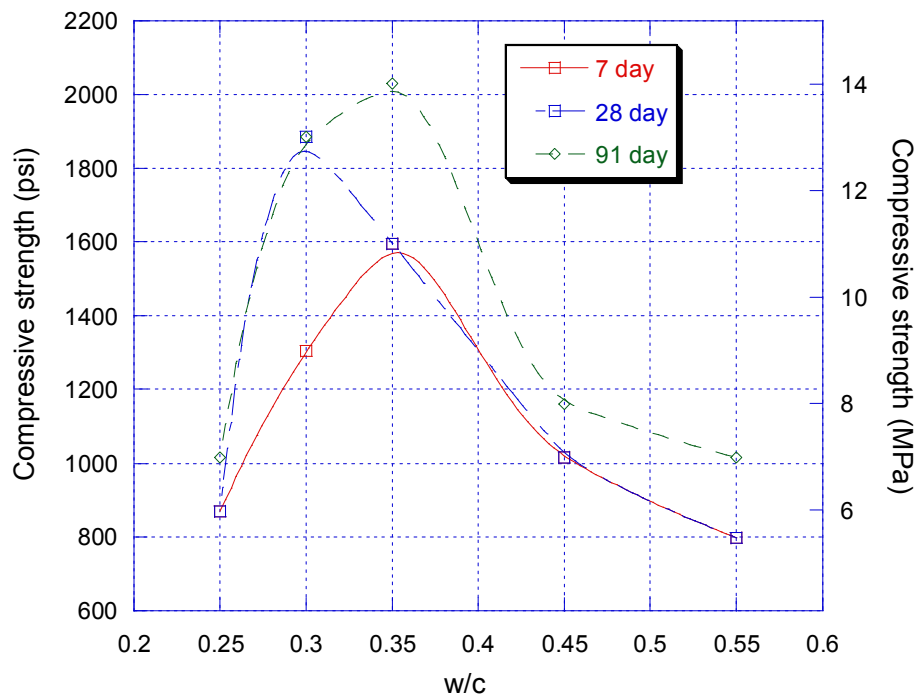


Figure 5 Relationship between w/c and compressive strength (cement content = 239 kg/m³), after Meininger (1988).

2.5.4 Cement Content

Figure 6 shows the relationship between compressive strength and cement content in water curing at 28 days. The compressive strength increases exponentially as cement content increases. Zouaghi et al. (2000) explained that the volume of cement paste

between aggregate particles controls bonding so that volume of cement paste strongly influences the compressive strength of pervious concrete.

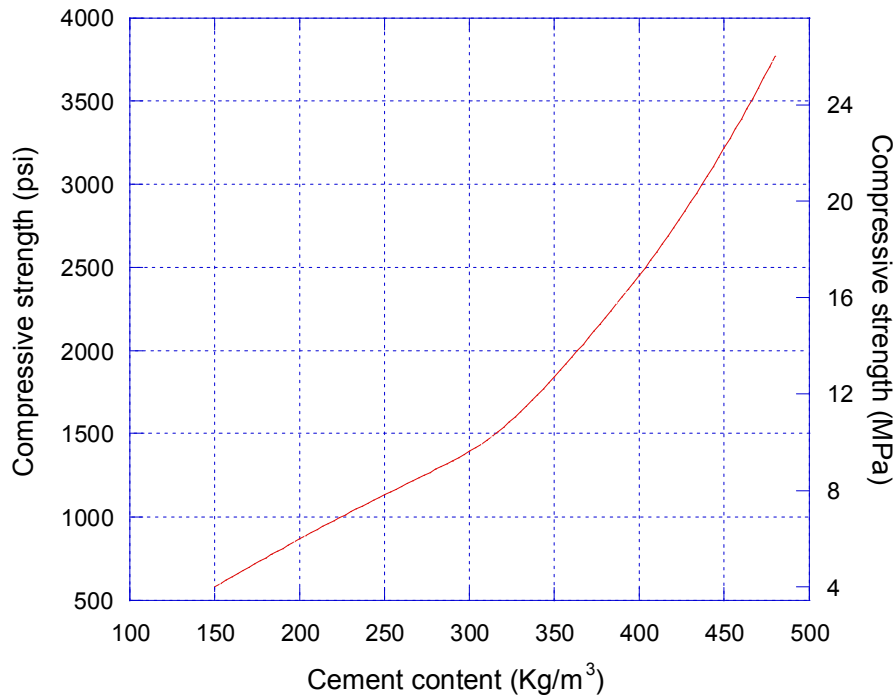


Figure 6 Relationship between compressive strength and cement content, after Zouaghi et al. (2000).

2.5.5 Sand

Mixtures including 10~20 % sand showed improved compressive strength (see Figure 7) and reduced air content versus those mixtures excluding sand entirely (Meininger, 1988). Added sand fills air voids, which increases density and compressive strength.

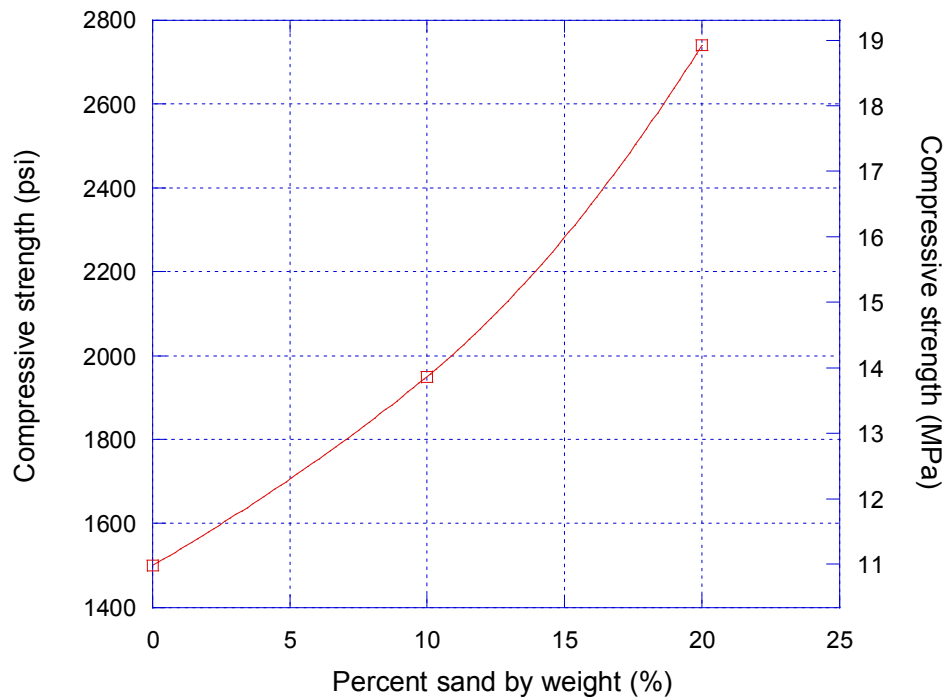


Figure 7 Relationship between sand content and compressive strength of pervious concrete, after Meininger (1988).

2.5.6 Silica Fume

Figure 8 shows the influence of silica fume on the compressive strength of pervious concrete. Counter to intuition, the addition of silica fume resulted in a reduction in the seven-day compressive strength by 44%. Schaefer et al (2006) explained that the silica fume influences the void ratio, and that the decrease of strength was due to increased void ratio caused by the presence of the silica fume. However, this report did not mention the usage of water-reducing admixtures in the mixtures. This Figure further emphasizes the point that air void content tends to dictate the compressive strength of pervious concrete.

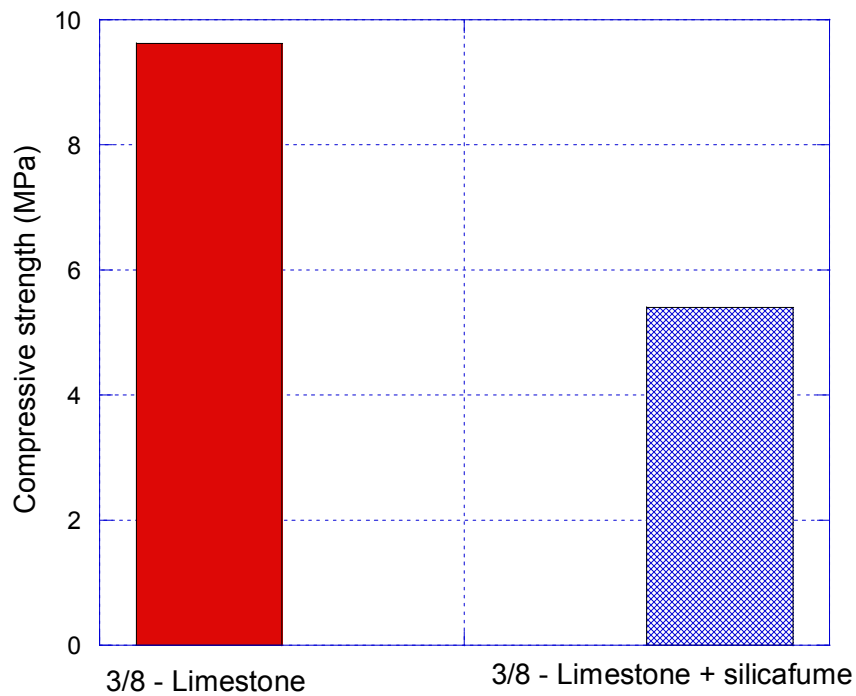


Figure 8 Effect of silica fume addition on the seven-day compressive strength of pervious concrete, after Schaefer et al. (2006).

2.5.7 Aggregate Size

Coarse aggregate grading in pervious concrete normally consists of either a single sized coarse aggregate or a narrow grading from 3/4 to 3/8 in. (19~9.5 mm) (ACI 522 pervious concrete, 2006). Though the range of coarse aggregate size was limited, Schaefer et al. (2006) briefly described the effect of aggregate size on compressive strength as shown in Figure 9.

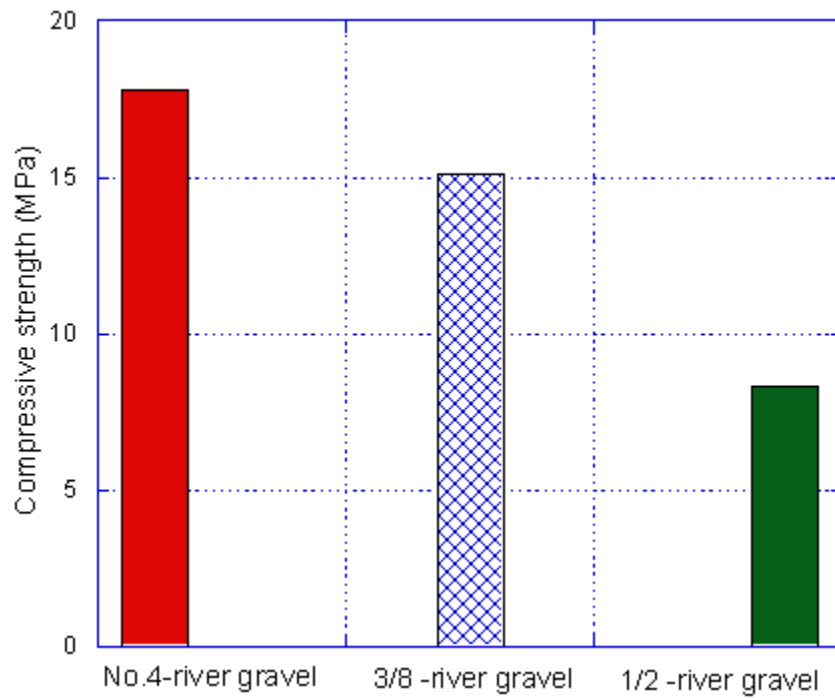


Figure 9 Effect of coarse aggregate size on compressive strength of pervious concrete, after Schaefer et al. (2006).

2.6 Flexural Strength

Several factors affect the flexural strength of pervious concrete. As expected, Figure 10 shows that flexural strength is reduced by increasing void ratio. Figure 11 indicates the relationship between flexural strength and the characteristic pore size (Marolf et al., 2004).

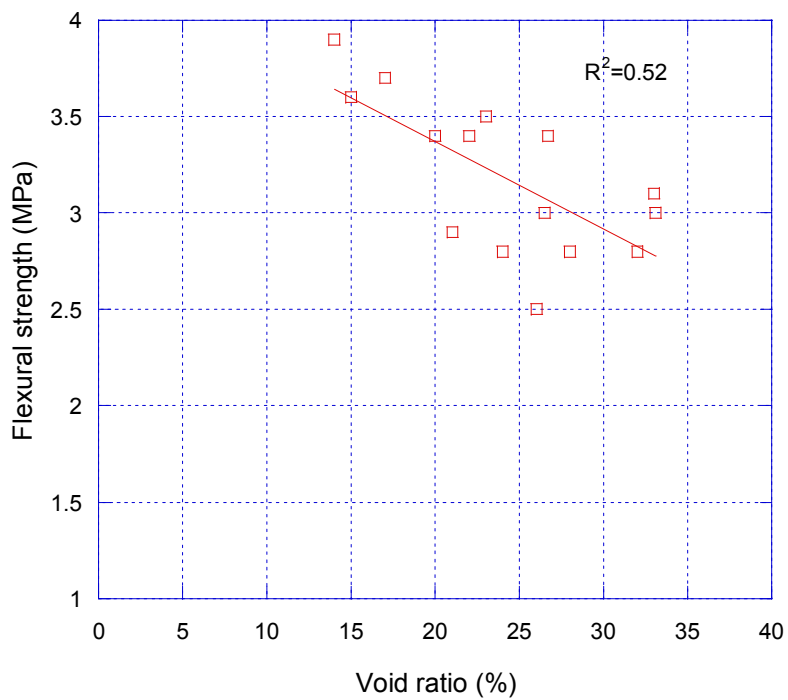


Figure 10 Relationship between flexural strength and total porosity, after Marolf et al. (2004).

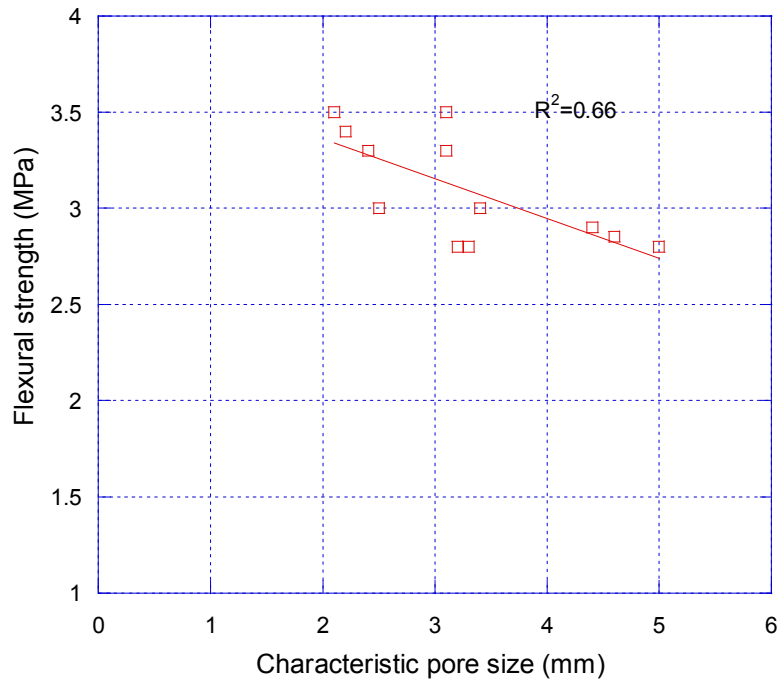


Figure 11 Relationship between flexural strength and characteristic pore size, after Marolf et al. (2004).

Figure 12 shows the relationship between compressive strength and flexural strength at the same void ratio. Based on the literature data, as void ratio increases, compressive strength tends to decrease more rapidly than flexural strength.

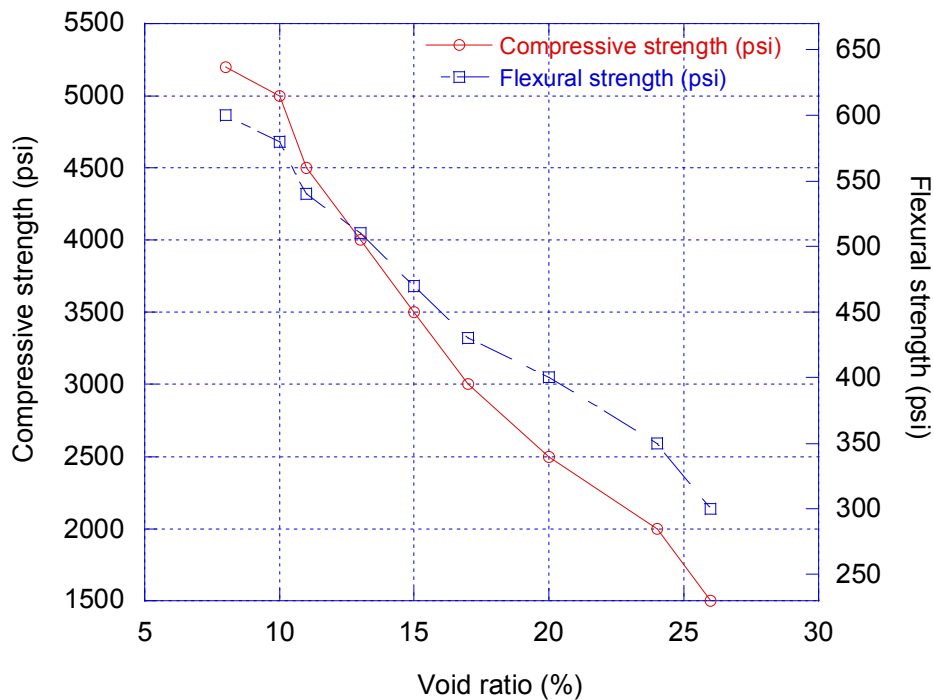


Figure 12 Comparison of the effect of void ratio on compressive and flexural strength using data from Meininger (1988).

2.7 Permeability

The most distinguished feature of pervious concrete is its high permeability, which is a measure of the ease by which fluid may flow through the material under a pressure gradient. Void ratio of typical pervious concrete ranges from 14% to 31% and permeability ranges from 0.0254 to 0.609 cm/sec (Schaefer et al., 2006). As one would expect, as the void ratio of pervious concrete increases, so does the permeability (see Figure 13).

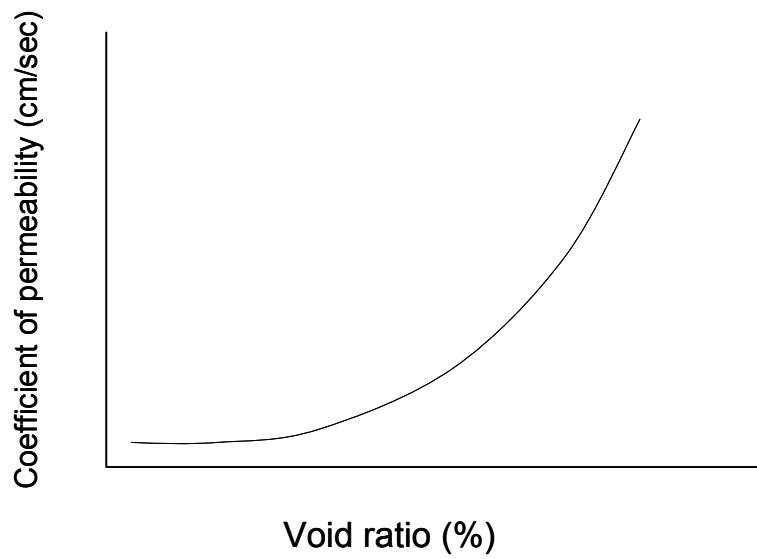


Figure 13 Relationship between pervious concrete void ratio and permeability for mixes placed using regular compaction energy, after Schaefer et al. (2006).

2.8 Clogging

Pervious concrete pavements are easily clogged by sand, dirt, and debris. Research on the clogging issue for pervious concrete is limited, but pervious asphalt clogging has been previously studied. Kraemer (1990) reported on the clogging of pervious asphalt in Europe. The initial drainage time of the unclogged concrete ranged from 25 to 75 seconds. After nine clogging cycles, drainage time increased from 160 to 400 seconds (Kraemer, 1990). As a primary function of pervious concrete is the ability to readily transport water, understanding the clogging issue of pervious concrete is essential for delineating future maintenance and for estimating the quality of pervious concrete pavement. Various methods to measure clogging of pervious pavements were implemented by Othman and Hardiman (2005), and Fwa et al.(1999).

Othman and Hardiman (2005) conducted clogging tests to determine the effect of particle size. Two kinds of particle sizes were investigated. Type A was a clayey soil, and Type B was a silty soil. Figure 14 shows the gradation of both types of soils. He mentioned that Type B took more time to clog the specimen than Type A since Type B was much coarser than Type A. Fwa et al. (1999) conducted tests to evaluate clogging of porous asphalt mixtures using a Type C soil.

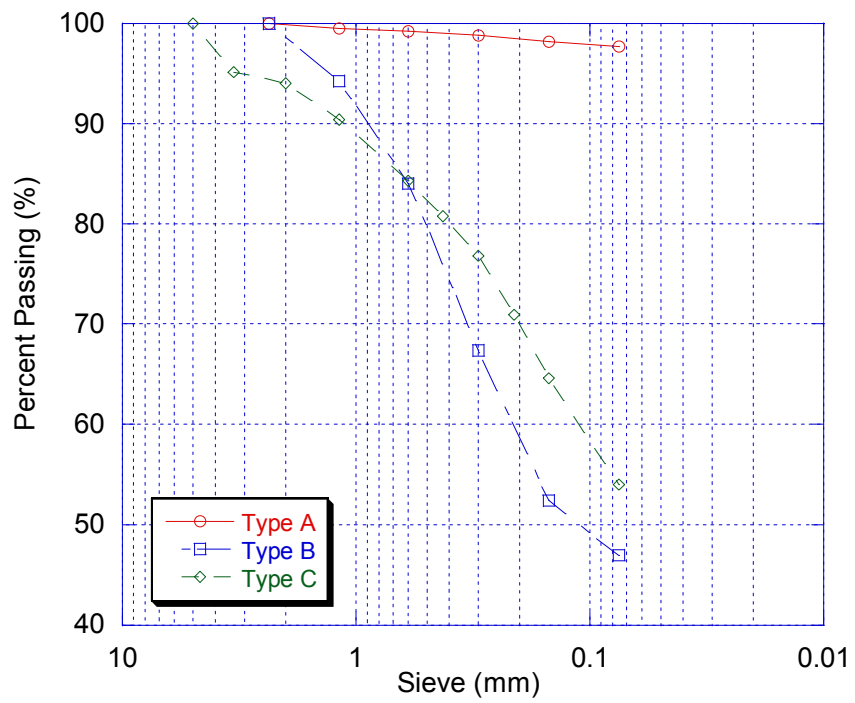


Figure 14 Gradation of type A ,B, and C after Othman and Hardiman (2005); Fwa et al. (1999).

The procedure used by Fwa et al. (1999) for quantifying the effect of clogging on permeability is outlined below:

1. Place cylindrical specimen in a water-tight cylindrical container with a water outlet at the bottom.
2. Put 35 g of the sand over the top of sample.
3. Pour 2 liters of water from the top of the cylinder.
4. Repeat step 2 nine times
5. After removing residual sand on the top of the sample, do permeability test.
6. Repeat steps one to five until the difference of the measured permeability is minimal (Fwa, et al. 1999)

Figure 15 shows the relationship between mass of clogging soil and permeability. Using binder Type A, clogging reduces the permeability from 2.5 to 0.4 cm/sec; using binder Type B the permeability decreases from 1.5 to 0.2 cm/sec.

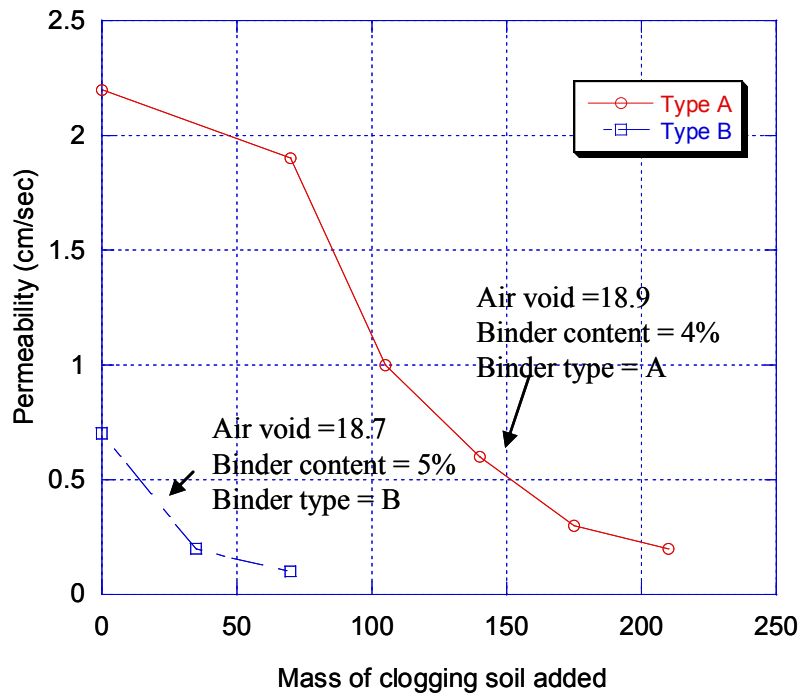


Figure 15 Relationship between mass of clogging soil and permeability in asphalt porous friction course pavement material using data from Fwa, et al. (1999).

2.9 Mixture Proportion

Various mixture proportions of pervious concrete have been studied for various research purposes. All mixture proportions are in a similar range. Pervious concrete contains minimal fine-aggregate so that large amounts of coarse aggregate are used compared with mixture proportion of conventional concrete. Figure 16 shows the typical range of both fine and coarse aggregate in normal concrete and pervious concrete (Mulligan, 2005; Schaefer et al., 2006; Luck et al., 2006).

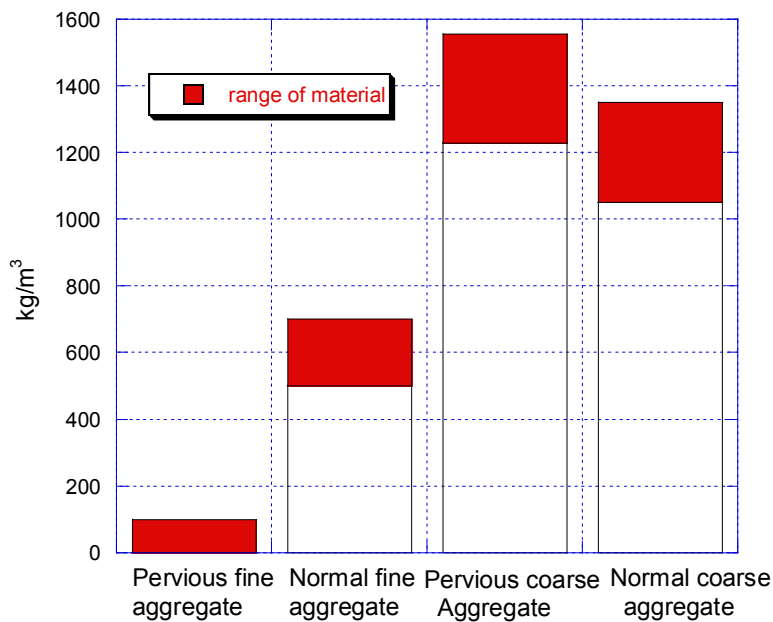


Figure 16 Comparison of typical range of aggregate proportions in pervious concrete mixtures versus approximate ACI normal concrete mixtures.

2.10 Pervious Concrete Pavement Design and Maintenance

2.10.1 Typical Cross-Section of Pervious Concrete

Pervious concrete pavement contains pores which allow rainfall to be captured so that pervious concrete pavement reduces runoff rapidly. Pervious concrete pavement typically contains two functional layers such as a finer upper layer, and a coarser bottom layer. The usage of functional layers has two benefits. First, the system of pervious concrete pavement is better at reducing traffic noise (Othman and Hardiman, 2005). Moreover, a finer pore structure at the pavement surface reduces clogging since the finer matrix does not allow problematic materials such as sand, dirt, and debris to deeply

penetrate through the pavement. A typical cross-section of pervious concrete is shown in Figure 17.

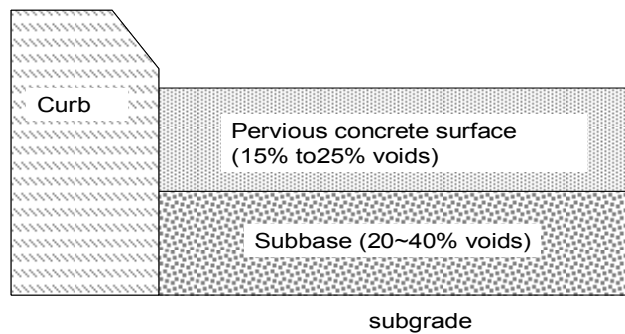


Figure 17 Typical cross-section of pervious concrete pavement, after Tennis et al. (2004).

2.10.2 Application of Pervious Concrete for Various Pavements

Pervious concrete pavements are typically used in several ways: driveways, parking lots, and (rarely) heavy traffic roads. The design of each is slightly different due to the different purposes. The type of sub-grade also influences the design; several types of soil sub-grades are classified including expansive and impervious sub-grade.

Figure 18 illustrates a standard parking lot or driveway pavement. Pervious surface pavement (four inches) covers a stone reservoir (eight inches). A non-woven geotextile fabric is placed at the bottom of the sub-base.

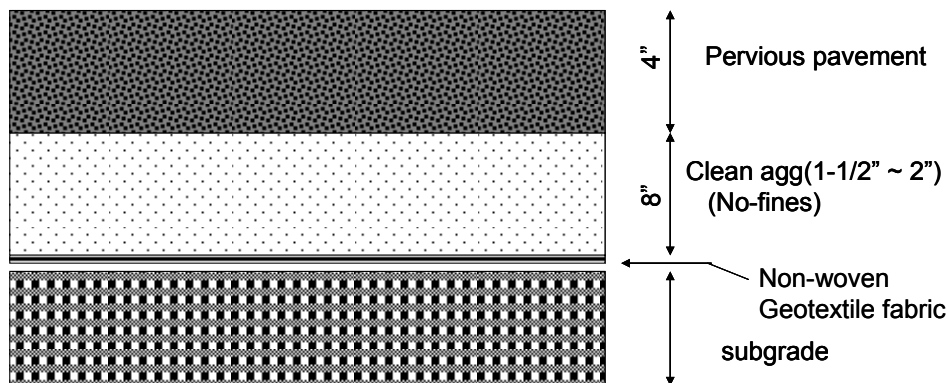


Figure 18 Typical parking & driveway pervious concrete pavement, after (www.stonecreekmaterials.com).

Figure 19 is a possible cross-section of a heavy traffic pervious concrete pavement. Both surface pavement and sub-base are thicker than for a standard pavement. The sub-base should be at least 10" thick. Non-woven geotextile fabric is located at the top of sub-grade. Figure 20 illustrates a typical concrete pavement cross-section for a normal sidewalk, cart path, hike, and bike trails.

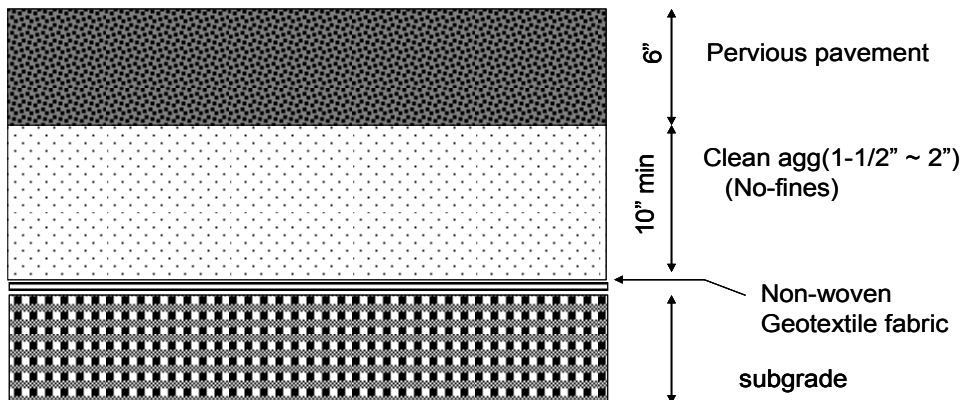


Figure 19 Pervious concrete pavement design for heavy traffic, after (www.stonecreekmaterials.com).

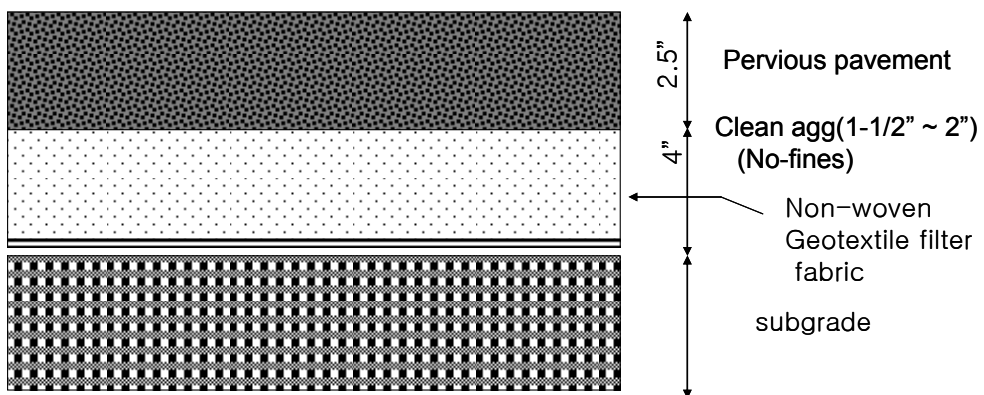


Figure 20 Pervious concrete pavement design for sidewalk, cart path, hike, and bike trails, after (www.stonecreekmaterials.com).

3 MATERIALS INVESTIGATION

3.1 Aggregate Properties

Two sizes of single-sized crushed limestone were used in this project. All of the coarse aggregate used in the study were sieved to obtain only single-sized aggregate. The two different sizes are listed below:

- 1/2 in. size (12.5 mm) with 100% passing the 5/8 in. and 100% retained on 1/2 in. sieve
- 3/8 in. size (9.5 mm) with 100% passing the 1/2 in. and 100% retained on 3/8 in. sieve.

Moisture content, absorption capacity, specific gravity, the rodded weight, and fineness modulus of the aggregates were measured with the results shown in Table 3. Figure 21 shows the gradation of the sand used in some of the mixtures.

Table 3 Properties of aggregate used in the pervious concrete mixes.

| | Fine aggregate | Coarse aggregate |
|------------------------------------|----------------|------------------|
| Specific gravity | 2.63 | 2.4 |
| Unit weight (lbs/ft ³) | - | 90 |
| Fineness modulus | 3.0 | - |
| Absorption capacity | 0.23 | 1.7 |

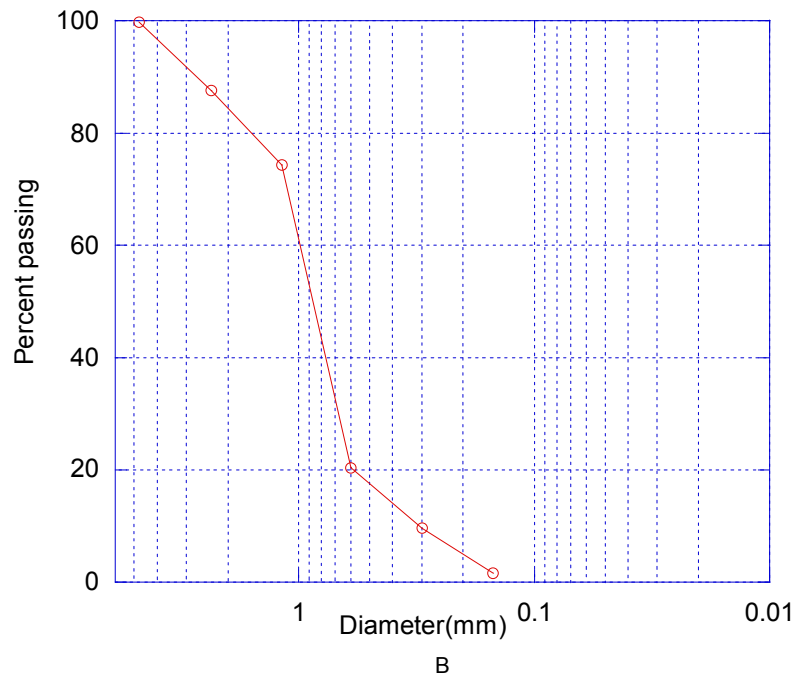


Figure 21 Gradation of sand used in this study.

3.2 Mixture Proportions

The mix design matrix was designed with three subsets, with mixtures in each subset designed to explicitly evaluate the effect of changing particular mixture proportions on the hardened properties of pervious concrete. The first subset of mixtures was designed to investigate how quantities of aggregate influence the void ratio and strength of pervious concrete. The second subset was designed to investigate how aggregate size, mixed aggregate, and cement content influence the void ratio and strength of pervious concrete. The third subset was designed to investigate the effects of cementitious materials (silica fume, class c fly ash), chemical admixtures (high range water reducer), and fibers (polypropylene fibers, steel fibers). The binder to aggregate ratio ranged from 0.12~0.40 and w/c was 30% through all mixtures. The proportions of all prepared mixes are shown in Table 4.

Table 4 Pervious concrete mixtures investigated in this study.

| Mix number | Agg.size (mm) | Binder | | | Agg. (kg/m ³) | Sand (kg/m ³) | Water (kg/m ³) | HRWR (oz per 100 lb PC) | w/c | Fibers | | Coarse agg. amount | Fine agg. amount | |
|------------|------------------|--------------------------------|-------------------------------------|-----------------------------------|---------------------------|---------------------------|-------------------------------|-------------------------------|------|--------|-------|--------------------------|---------------------|------|
| | | Cement (kg/m ³) | Silica fume (kg/m ³) | Fly ash C (kg/m ³) | | | | | | Poly | Steel | | | |
| Type 1 | No.1 | 12.5 | 189.5 | – | – | 1564.6 | 0 | 56.1 | – | 0.3 | – | – | High | Low |
| | No.2 | 12.5 | 275 | – | – | 1396.0 | 50.0 | 82.7 | – | 0.3 | – | – | Mid | Mid |
| | No.3 | 12.5 | 357.8 | – | – | 1227.0 | 99.1 | 106.8 | – | 0.3 | – | – | Low | high |
| Type 2 | No.3-1 | 9.5 | 357.8 | – | – | 1227.0 | 99.1 | 106.8 | – | 0.3 | – | – | Low | high |
| | No.3-2 | 9.5+12.5 | 357.8 | – | – | 1227.0 | 99.1 | 106.8 | – | 0.3 | – | – | Low | high |
| | No.3-3 | 9.5 | 465.2 | – | – | 1069 | 99.1 | 138.8 | – | 0.3 | – | – | Low | high |
| Type 3 | No.4 | 12.5 | 340 | 17.9 | – | 1227.0 | 99.1 | 107.8 | – | 0.3 | – | – | Low | high |
| | No.4-1 | 12.5 | 340 | 17.9 | – | 1227.0 | 99.1 | 107.8 | 30.0 | 0.3 | – | – | Low | high |
| | No.5 | 12.5 | 286 | – | 71.6 | 1227.0 | 99.1 | 107.8 | – | 0.3 | – | – | Low | high |
| | No.6 | 12.5 | 357.8 | – | – | 1227.0 | 99.1 | 106.8 | – | 0.3 | used | – | Low | high |
| | No.7 | 12.5 | 357.8 | – | – | 1227.0 | 99.1 | 106.8 | – | 0.3 | – | used | Low | high |

3.3 Specimen Preparation

Initial pervious concrete samples such as 4 in. diameter x 8 in. height cylinders, 6 in. diameter x 12 in. height cylinders, and 6 in. x 6 in. x 18 in. beams were prepared by using a standard concrete mixing procedure. Before mixing the concrete, the rotating drum mixer was ‘battered’ with water. Then, the mixer was stopped for five minutes to drain excess water. Next, coarse aggregate and half the measured water were added to the mixer. The fine aggregate and cementitious materials were slowly added into the rotating drum mixer. Finally, the remaining half of the water was added. Mixing continued for three minutes from start time. Then, the mixer was stopped for three minutes, and finally run for an additional three minutes. All of the cylindrical specimens in this study were placed by rodding 25 times with tamping rod in three layers. The outside of the molds was lightly tapped 15 times with a mallet. The beam mold was filled with concrete in two layers and each layer was tamped 50 times. The samples were subsequently demolded after 24 hours and placed to cure in 100% relative humidity conditions.

Cylinders 4 in. diameter x 8 in. height were used for compressive strength tests, air content tests, and ‘dynamic pressurization’ tests (see Section 6). Cylinders 6 in. diameter x 12 in. length were used for permeability tests. Beams with a cross-section of 6 in. x 6 in. and a length of 16 in. were used for flexural strength.

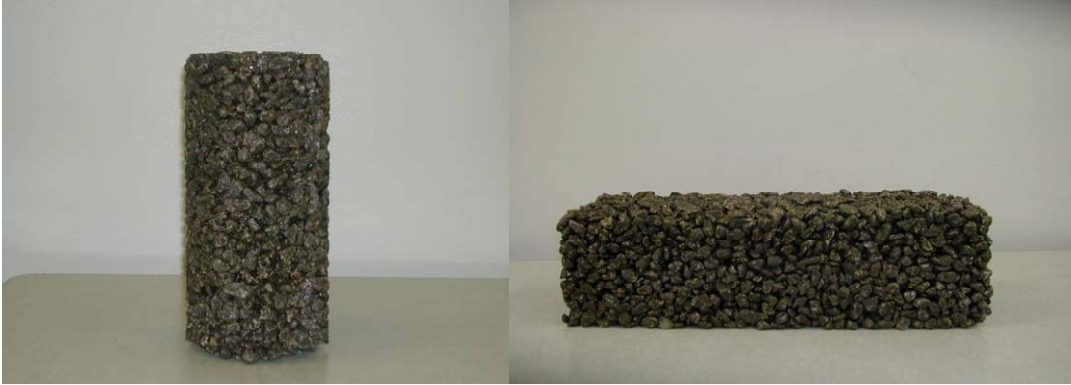


Figure 22 6 in. x 12 in. cylindrical sample and 6 in. x 6 in. x 18 in. beam sample.

4 EFFECT OF MIXTURE DESIGN ON STRENGTH OF PERVIOUS CONCRETE

4.1 *Testing Procedures*

4.1.1 Standard Tests

Several standard tests were performed to determine the characteristics of pervious concrete such as slump, air content, unit weight, compressive strength, and flexural strength. Slump tests were performed according to ASTM C143, and unit weight was measured according to ASTM C29. The compressive strength was measured according to ASTM C39, and flexural strength was measured according to ASTM C78.

4.1.2 Air Content Test

The air void content of pervious concrete can not be measured using an typical test such as ASTM C173 since the capacity of the air meter is not large enough to measure the high air void contents of pervious concrete. Therefore, the air void content of pervious concrete was calculated by using the difference of weight between the air dry sample and the saturated sample under water. Equation (1) (Park and Tia, 2004) was used in this test:

$$V = \left[1 - \left(\frac{W_2 - W_1}{\rho_w Vol} \right) \right] \times 100\% \dots\dots\dots (1)$$

where V is the total percent air void content, W_1 is the mass of the saturated sample, W_2 is the mass of the oven dry sample, Vol is the volume of the sample, and ρ_w is the density of water.

A summary of the test procedure is listed below:

1. Measure the external volume of the sample
2. Measure mass of oven dried sample
3. Measure the mass of the saturated sample
4. Use Equation (1) to determine V .

4.2 Results

4.2.1 Effect of Aggregate Content

The slump of all the pervious concrete mixtures measured from 0 to 1 in., except for two mixtures which had a high amount of coarse aggregate, and middle amount of coarse aggregate (see Table 4). Specimens (see Figure 23) made with mixtures from the Type 1 (Table 4) subset were batched on the basis of volume of coarse aggregate. As the amount of coarse aggregate increases, the cement paste volume decreases which results in a weaker bonding between the aggregates (Figure 24). Inter-aggregate bonding is critical for the strength of pervious concrete, and therefore the strength of pervious concrete is strongly dependent on the thickness of paste layers coating the aggregate particles. The paste coating thickness is directly dependent on the coarse aggregate content. Figure 25 shows the effect of the coarse aggregate content on measured compressive strength.



Figure 23 Picture of samples (from left to right, low coarse aggregate, mid coarse aggregate, and high coarse aggregate).

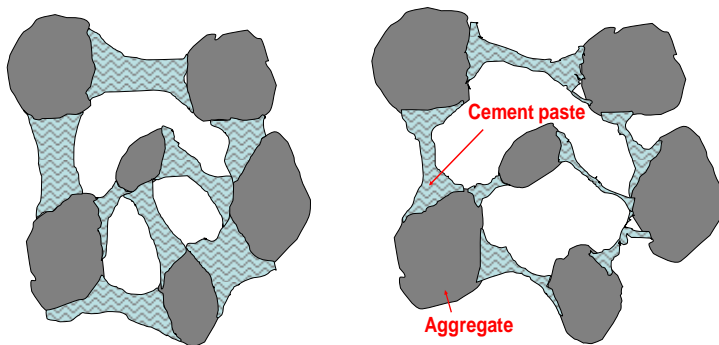


Figure 24 Higher paste content (left) and lower paste content (right). As volume of coarse aggregate increases, volume of paste decrease.

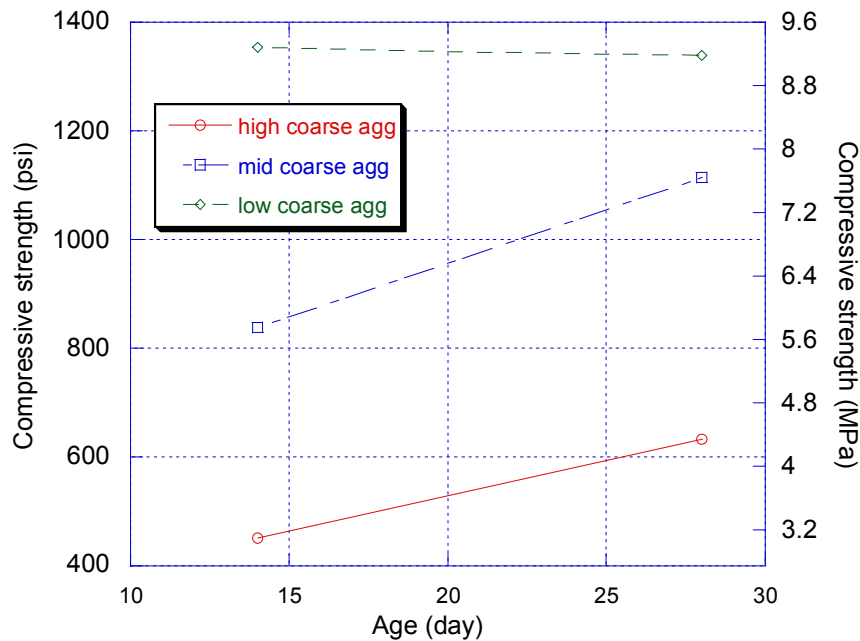


Figure 25 Effect of coarse aggregate content on compressive strength evolution (high coarse agg = high volume of coarse aggregate, mid coarse agg = middle amount of coarse aggregate, low coarse agg = low volume of coarse aggregate).

4.2.2 Effect of Cementitious Materials and Aggregate Size

The use of materials such as class C fly ash or an increase in the cement content used in pervious concrete mixtures will increase compressive strength. A smaller single size coarse aggregate such as 9.5 mm (versus 12 mm) used in pervious concrete shows no increase of 28-day compressive strength, however smaller size coarse aggregate combined with higher cement content shows that 28-day compressive strength was improved by 35%. The mixtures that yielded the highest compressive strength of those tested contained class C fly ash and higher cement content, which resulted in the lowest void ratio. The void ratio of the fly ash mixtures was 22%, and the void content of the

higher cement content mixture was 18%, compared to 31% void ratio of the standard mixture. On the other hand, the mixture with a combination of two aggregate sizes (9.5 mm +12.5 mm) did not show an increase of compressive strength, and neither silica fume nor silica fume with HRWR improved compressive strength in comparison to the standard mixture (No.3).

Compressive strength of the mixtures with the combination of two aggregate sizes (No.3-2) ranged from 857 to 1467 psi. The Coefficient of Variation (COV) was 0.186. Since compaction of pervious concrete is critical to low variability in pervious concrete strength, it may be that some samples were not as fully compacted as others, as suggested by visual observation of the various pervious concrete cylinders (see Figure 26, Figure 27). In the Figures, white marked circles show poorly compacted zones that resulted in small gaps between aggregates. Therefore, these samples may have had a slight increase in the void ratio due to poor compaction. When silica fume was added to mix, compressive strength decreased primarily due to workability problems. The addition of silica fume negatively affected workability, which caused compaction problems, and did not allow the cement paste to uniformly coat the aggregate particles. Figure 28 and Figure 29 show the results of the compressive strength measurements of the relevant samples.



Figure 26 The top of sample incorporating both 9.5 mm and 12.5 mm aggregates.
The white circle indicates a region of poor compaction.



Figure 27 The side of sample incorporating both 9.5 mm and 12.5 mm aggregates.
The white circles indicate regions of poor compaction.

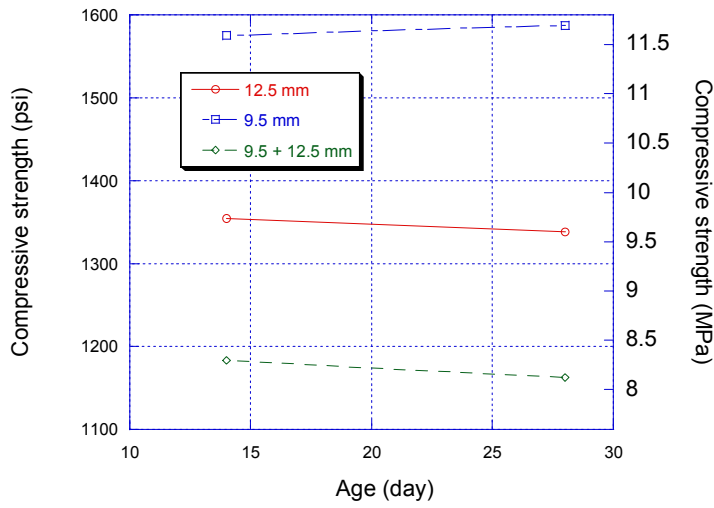


Figure 28 Effect of aggregate size on compressive strength.

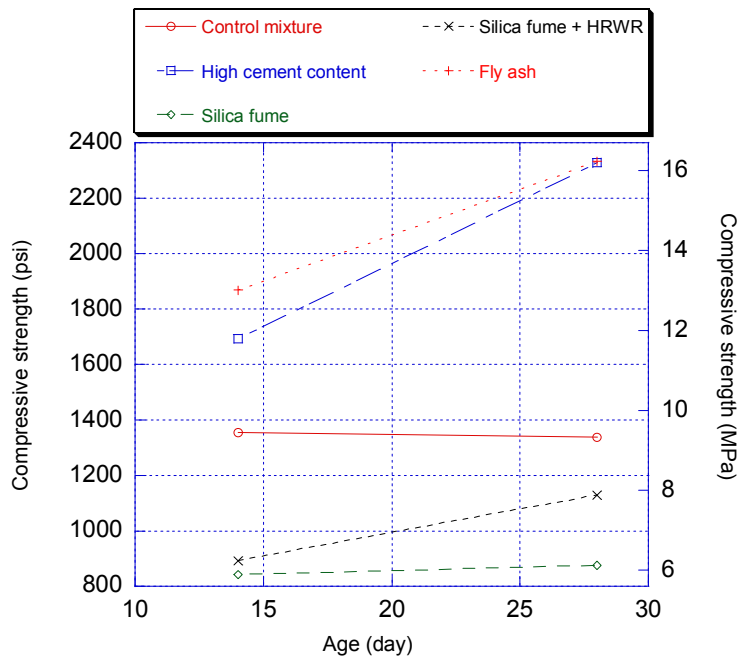


Figure 29 Effect of cementitious materials on compressive strength.

4.2.3 Effect of Void Ratio on Compressive Strength

Figure 30 shows the relationship between the measured void ratio and compressive strength. The void ratio of the pervious concrete specimens tested ranged from 15% to 35% at 28 days. According to ACI 522R-7 report, the void ratio is strongly dependant on aggregate gradation, cementitious materials content, w/c, and compaction effort. In this study, two kinds of aggregate gradation and different cementitious materials were investigated. The standard sample, mixture No.3, had an average void ratio of 31%. The mixture using small size coarse aggregate (No.3-1) had an average measured void ratio of 23%, and the mixture with a combination of aggregate sizes (No.3-2) had a void ratio of 25%. The results show that the void ratio is dependent on the aggregate size. Smaller aggregates tend to pack more efficiently yielding reduced void space. After supplementary cementitious materials were added to the concrete mixtures, the results were varied. Using silica fume or silica fume with HRWR did not reduce void ratio, however class C fly ash shows significant decrease of the void ratio. While mixing materials with silica fume, it was noted that a large amount of paste would adhere to the mixer. It is possible that a portion of this paste was not able to be recovered, resulting in a slight reduction in actual paste content in the cast specimens.

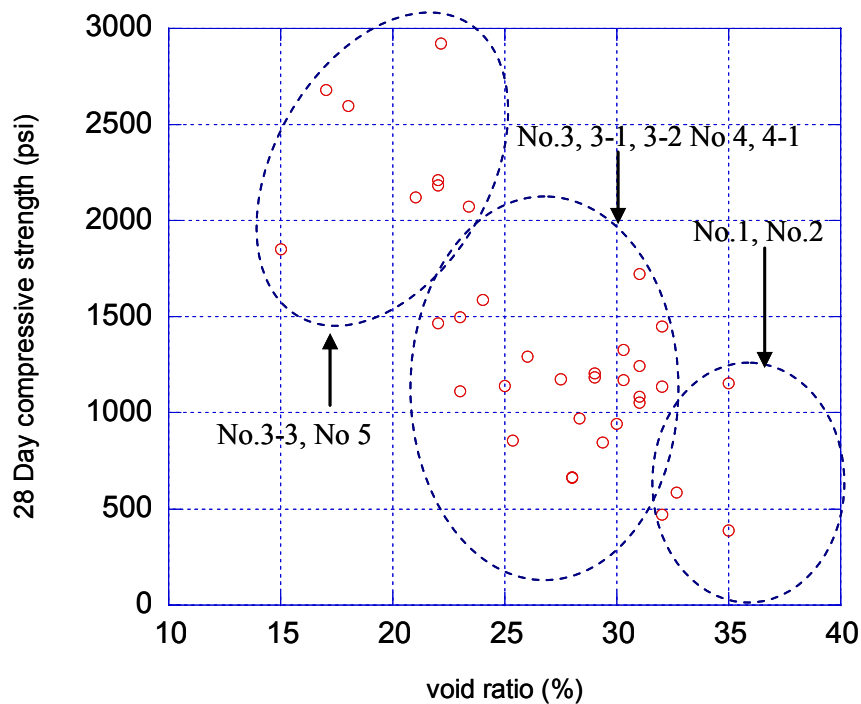


Figure 30 Relationship between void ratio and 28-day compressive strength. The numbers in the Figure denote different mixtures as shown in Table 4.

4.2.4 Effect of Void Ratio and Fiber Reinforcement on Flexural Strength

Concrete pavements are normally loaded such that the pavement is in a condition of two-dimensional flexure. Therefore, while compressive strength is the most common measure of a paving material's structural capacity, flexural strength gives a more appropriate measure of the resistance of a paving material to structural failure.

Compressive strength and flexural strength are, for the most part, similarly dependent on the same mixture criteria. However, fiber reinforcement tends to have a minimal effect on compressive strength of normal concrete but a significant effect on the flexural strength of normal concrete. Therefore, in the interest of discovering methods for

improving the structural performance of pervious concrete, the effect of fibers on the flexural strength was investigated.

Figure 31 shows the relationship between flexural strength and air void ratio. As expected, as the air void ratio decreases, flexural strength increases. Polypropylene and steel fibers were added to pervious concrete mixtures to evaluate their effect on flexural strength, but the results indicate these fibers do not substantially improve flexural strength.

According to the photographs of the fiber-reinforced samples (see Figure 32), several porous spaces between the coarse aggregate particles are filled with fibers. It is hypothesized that the fibers did not contribute substantially to the flexural strength of pervious concrete because the fibers were covered with only a thin layer of paste (over a minimal length of the fiber) such that the bonding was poor. This allowed fibers to pull out at low stress levels. Figure 33 illustrates this concept.

When smaller coarse aggregates and the combination of two aggregate sizes were used, flexural strengths were higher than samples using fibers. Beams containing smaller or mixed size coarse aggregate has less space between aggregates, which allows a greater contact area between the paste coatings on each individual aggregate particle (see Figure 34). Therefore, using a smaller coarse aggregate (or a broader range of aggregate sizes) will influence the flexural strength of pervious concrete more than the use of fibers.

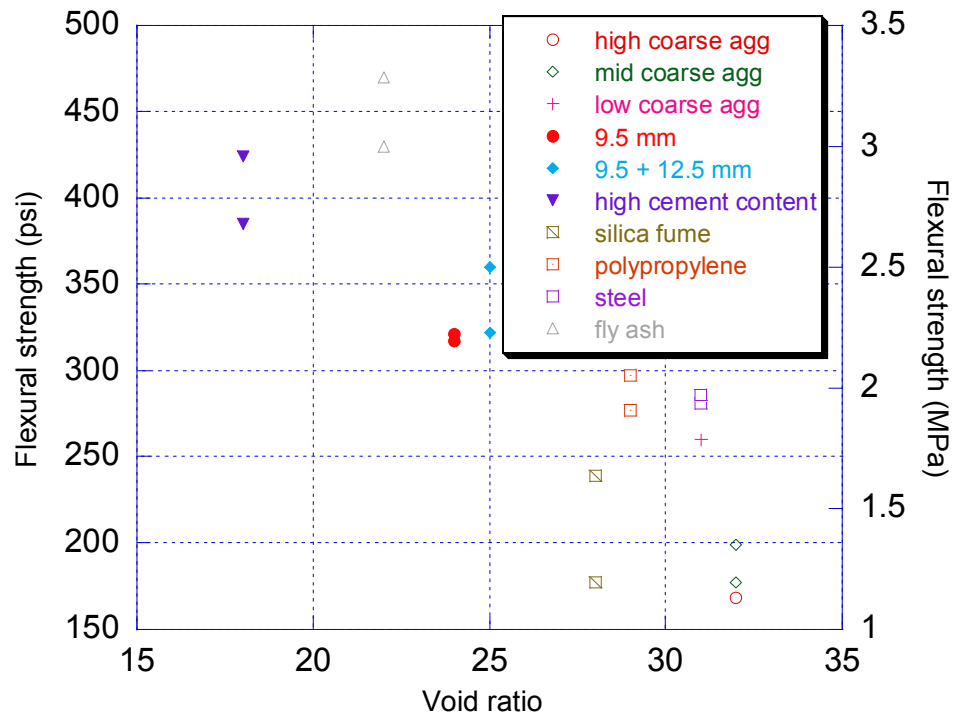


Figure 31 Relationship between void ratio and flexural strength.



Figure 32 6 in. x 6 in. x 12 in. beam sample after flexural test (polypropylene).

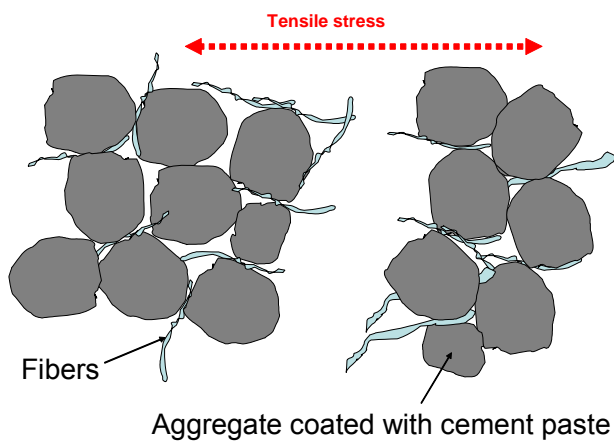


Figure 33 Illustration of why addition of fibers does not significantly increase flexural strength. Since bonding is poor, fibers are not strongly bonded to paste so that even low stress leads fibers to pull out.

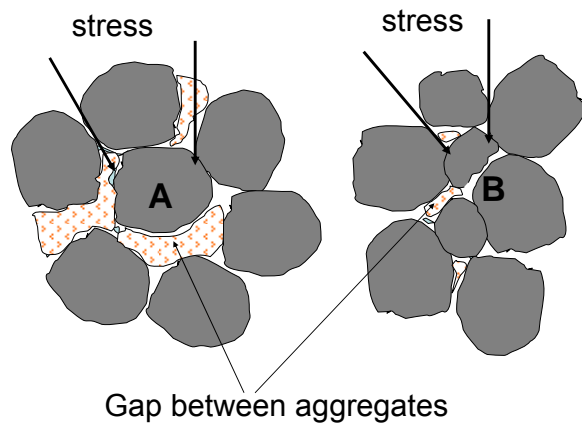


Figure 34 Comparison of the inter-aggregate gap in mixtures using 12.5 mm aggregate (A) or a combination of 9.5 mm and 12.5 mm (B). The large space between aggregates in (A) leads pervious concrete beam to easily fail in tension.

4.2.5 Effect of Unit Weight on Compressive, Flexural Strength

As expected by the results relating the compressive and flexural strength to the void ratio, the compressive and flexural strength of pervious concrete both increase as a function of unit weight. A larger unit weight implies a reduced void ratio (see Figure 35, Figure 36, and Figure 37). The results of this study agree well with those found in the literature, as listed in Table 1.

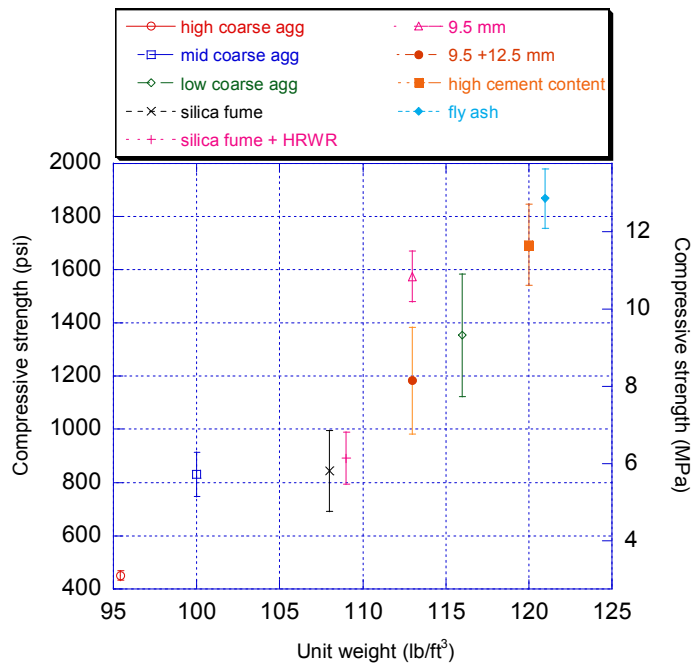


Figure 35 Relationship between 14-day compressive strength and unit weight.

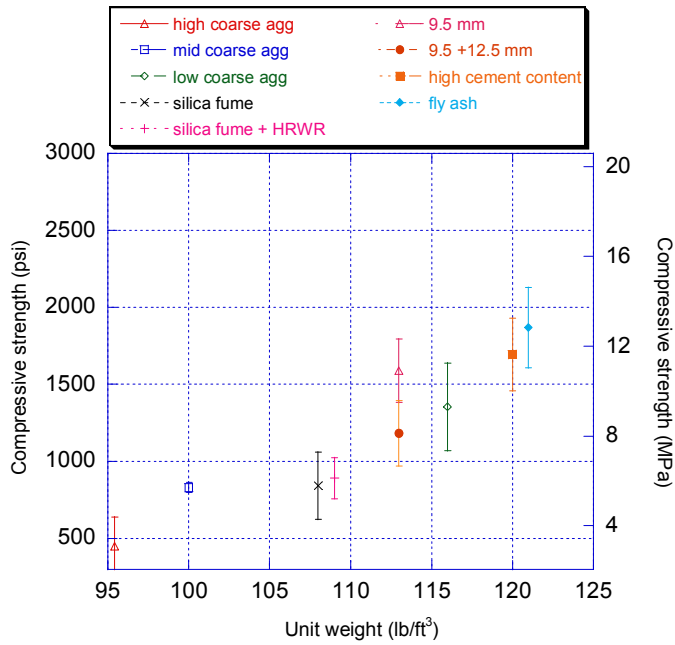


Figure 36 Relationship between 28-day compressive strength and unit weight.

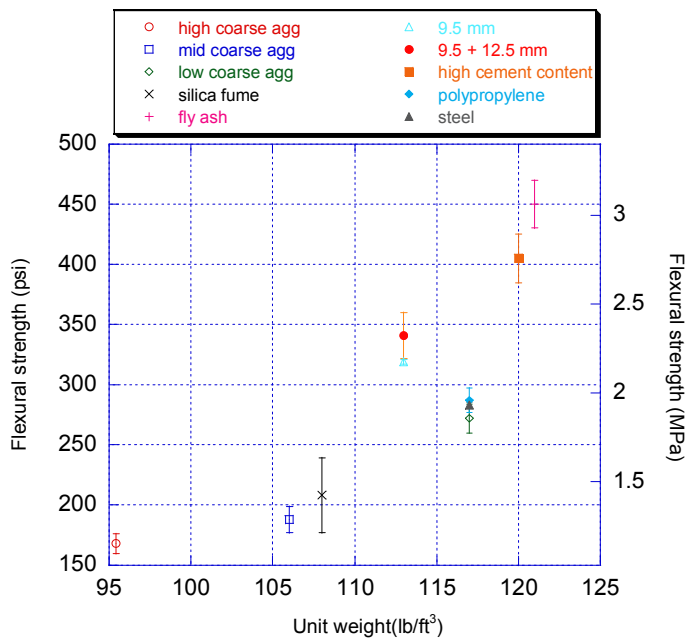


Figure 37 Relationship between flexural strength and unit weight.

5 EFFECT OF MIXTURE DESIGN ON PERMEABILITY AND CLOGGING OF PERVIOUS CONCRETE

5.1 Permeability Measurement

The permeability of the various pervious concrete mixtures described in Table 4 was determined using the falling-head permeability test apparatus illustrated in Figure 38.

The coefficient of permeability (k) was determined applying Equation (2):

$$k = \frac{aL}{At} \log e \left(\frac{h_1}{h_2} \right) \dots\dots\dots (2)$$

where k is the coefficient of water permeability, a is cross-sectional area of the standpipe, L is the length of the sample, A is the cross-sectional area of the specimen, and t is the time for water to drop from level h_1 to h_2 (Das, 1998).

A summary of the test procedure is outlined below:

1. Vacuum air inside air tube, set the sample into the equipment
2. Pour water into the sample, then put some air into air tube to compress the sides of the sample eliminating the potential for leaks
3. Remove air bubbles using vacuum
4. Fill equipment with water up to initial water level (h_1). Then, drain water
5. Repeat step four five times
6. Measure time while water level decreases from initial level (h_1) to final level (h_2)

7. Repeat step six five times, then obtain average.

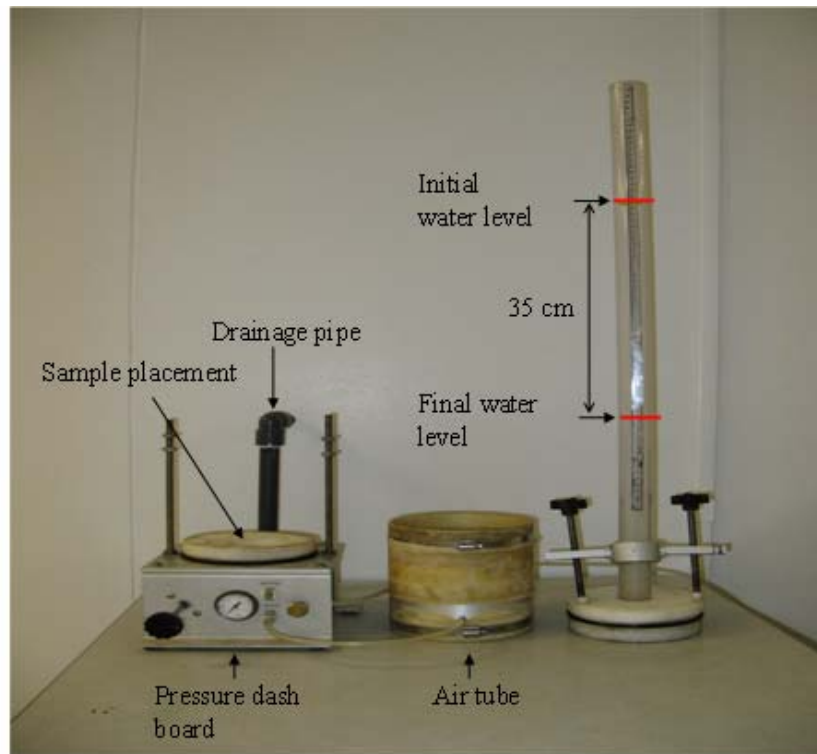


Figure 38 Falling-head permeameter used to measure coefficient of permeability of pervious concrete.

5.2 Clogging Test

After the permeability of each pervious concrete mixture was measured, a clogging test was performed. The clogging test allowed evaluation of the change in permeability as a function of clogging material added to the pervious concrete using Equation (2). The clogging procedure used in this research is summarized below:

1. Place 50 g of the clogging material (sand) per 1 kg water in a bucket and mix thoroughly
2. Pour clogging fluid into the ready sample in the clogging apparatus shown in Figure 39
3. Drain mixed water from the cylinder
4. Repeat step 1, 2 five times such that the pervious concrete cylinder becomes well clogged with sand
5. Set the clogged sample in the falling-head permeameter (Figure 38)
6. Measure the time for the water head to fall from initial level to final level while draining. Repeat five times and average the results.



Figure 39 Device used to clog pervious concrete cylinders using sand/water mixture.

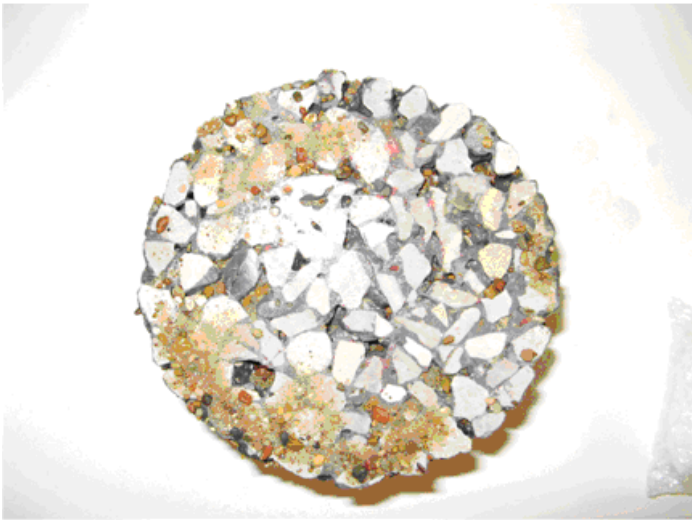


Figure 40 Clogged sample after clogging test. Sand is present in pores, and excessive sand is apparent on the surface of the sample.

5.3 Results

5.3.1 Void Ratio and Coefficient of Permeability

Figure 41 shows that the coefficient of permeability of all pervious concrete mixtures was improved as a function of void ratio. At void ratios above 23%, the permeability sharply increases. For all mixes, the coefficient of permeability ranges from 0.02 to 0.46 cm/sec. The mixes with the maximum coefficient contain class C fly ash and high volume of coarse aggregate. Low permeability mixes are those with high cement content. In addition, mixtures containing silica fume with HRWR tend to have a lower permeability in comparison to other mixes. Mixtures containing fly ash show abnormally high permeability with respect to the void ratio; it is possible that for some reason the fly ash concrete has a less tortuous pore geometry that yields the higher permeability with respect to the void ratio.

According to the report of historical extreme rainfall events (Carter, 1975), in Austin, TX the highest rainfall intensity was 0.0035 cm/sec (duration in an hour) during a 100 year return period. Therefore, all mixes prepared in this study can deal with extreme rainfall event (assuming no clogging is present). It is likely that mixtures used in this study were over-designed for permeability. In other words, mixtures could have been designed with a lower permeability but with higher compressive and flexural strength since there is typically a trade-off between these two properties. Since the permeability (0.02cm/sec) of even the high cement content pervious concrete is higher than permeability of the most extreme rainfall events (0.0035cm/sec), that mixture is likely to

be the best performing in terms of balancing strength and permeability. Figure 42 shows the relationship between permeability and 28-day compressive strength (f'_c).

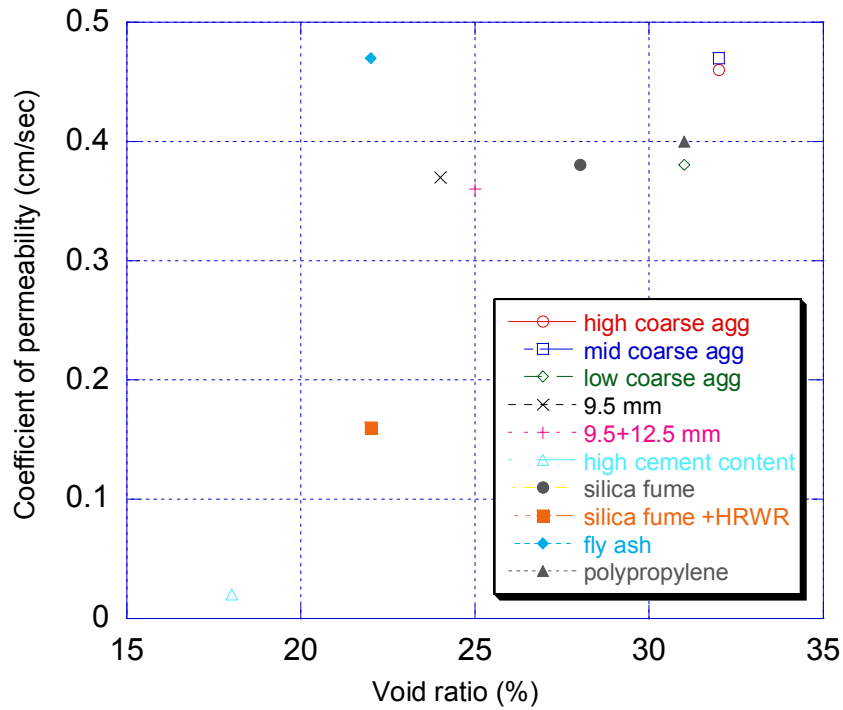


Figure 41 Relationship between void ratio and coefficient of permeability for all mixtures.

aggregate and middle amount of coarse aggregate have an extremely high coefficient of permeability.

Figure 43 shows that the low amount of coarse aggregate pervious concrete (using 12.5 mm aggregate) has a similar coefficient of permeability to the pervious concrete using smaller coarse aggregate (9.5 mm). Both samples have similar void ratio.

Those pervious concrete specimens with a void ratio over 33% (such as high and middle amount of coarse aggregate pervious concretes) were not affected by clogging sand, however those specimens with a void ratio ranging from 31 to 23% were affected by clogging sand. The largest incremental decrease of permeability occurred after the first clogging cycle.

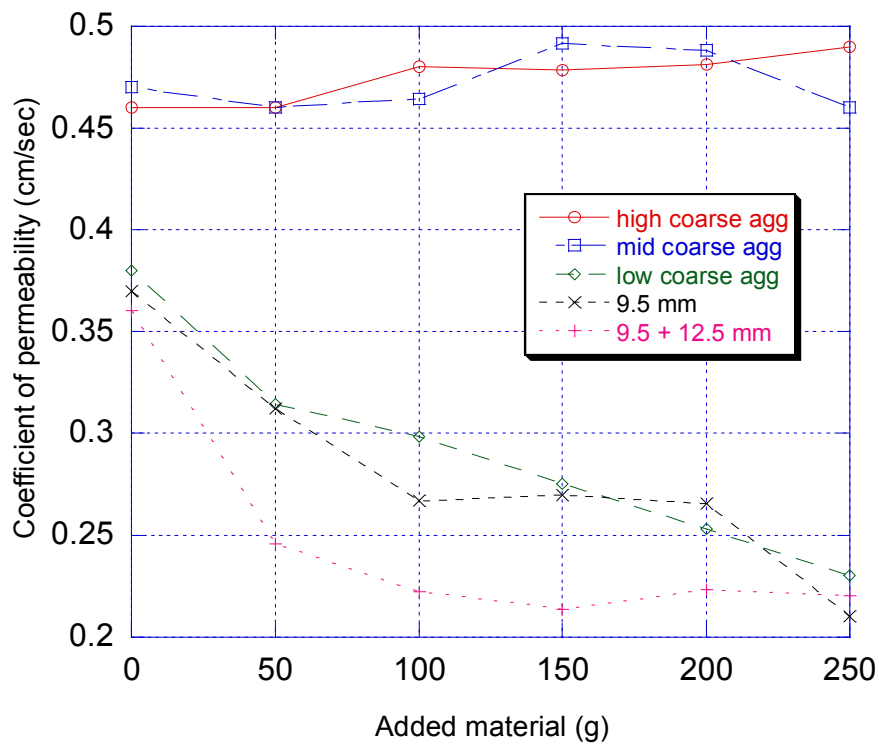


Figure 43 Relationship between amount of clogging material added to the specimens and coefficient of permeability. High coarse agg (12.5 mm) = high volume of coarse aggregate, mid coarse agg (12.5 mm) = middle volume of coarse aggregate, low coarse agg (12.5 mm) = low volume of coarse aggregate.

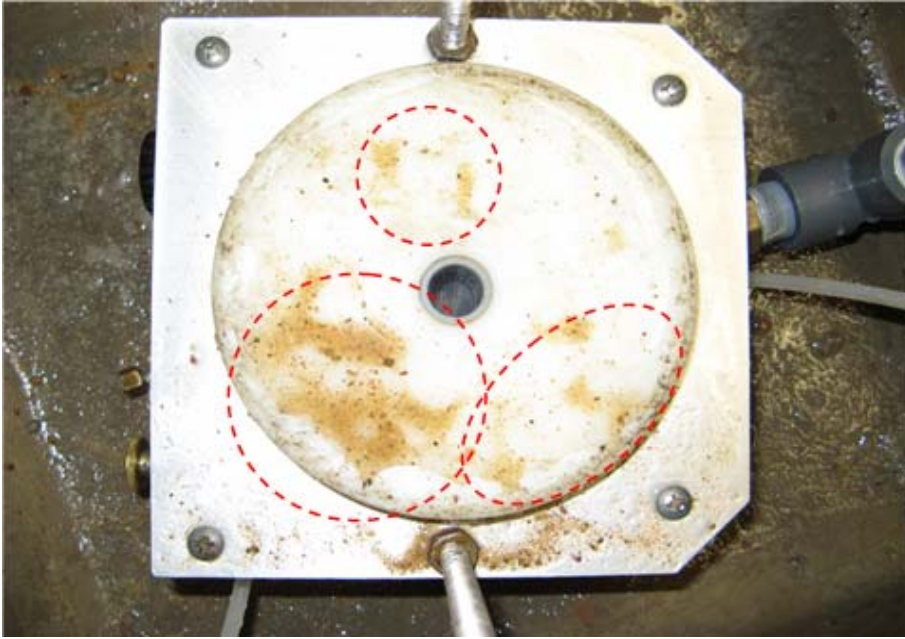


Figure 44 Sand flushed from sample after clogging test. Marked circles show sand that was flushed out during the permeability test.

6 EVALUATION OF DYNAMIC PRESSURIZATION TEST TO EVALUATE DURABILITY OF PERVIOUS CONCRETE

6.1 Motivation

Permeability is the principle parameter chosen to quantify the durability of concrete. Since deterioration in concrete is linked to the movement of moisture, permeability is a suitable choice to evaluate durability in normal concrete. Several experiments have been developed to measure concrete permeability and are summarized in (Grasley, 2006).

All existing tests to quantify permeability of traditional concrete are incapable of assessing durability of pervious concrete. Durability is dictated by the nano-micro pore structure of the paste layers coating the aggregate particles. The result of rapid chloride permeability test and flow-through test parameters are dictated by the macro-porosity, which is intended to be maximized in pervious concrete to optimize the material function as a pervious concrete pavement. The test technique to be described in the following sections does not measure the overall bulk flow rate of fluid through pervious concrete, but rather allows the measurement of the flow rate of fluid into the nano-micro pore structure of the paste layers which surround each aggregate. This allows for a potential quantification of the durability of pervious concrete as a function of the permeability of the paste layers coating the aggregate particles.

6.2 DP Test Theory and Introduction

The Dynamic Pressurization (DP) test technique involves placing a saturated concrete cylinder under a constant hydrostatic pressure. The cylinder will initially contract under the pressure, but will gradually re-expand as the pressurized fluid flows into the pore network. The rate of re-expansion of the cylinder is related to rate of fluid flow in the pore network. Therefore, the rate of re-expansion is directly linked to the permeability of the specimen (Scherer, 2006).

The axial strain of a cylindrical sample following a step change in pressure is calculated by Scherer (2006).

$$\frac{\varepsilon_z(\theta) - \varepsilon_\infty}{\varepsilon_\infty - \varepsilon_0} = \Omega(\theta) \dots\dots\dots (3)$$

where $\Omega(\theta)$ is the hydrodynamic relaxation function. The initial strain induced by the applied pressure, p_A is

$$\varepsilon_0 = -\frac{P_A}{3K_p}(1 - b\lambda) \dots\dots\dots (4)$$

and the final strain is

$$\varepsilon_\infty = \frac{(b-1)P_A}{3K_p} = -\frac{P_A}{3K_s} \dots\dots\dots (5)$$

where K_p is the bulk modulus of the drained porous body, K_s is the bulk modulus of the solid material skeleton, $b = 1 - K_p / K_s$ is the Biot coefficient, $\lambda = Mb / (Mb^2 + K_p)$, and M is the Biot modulus,

$$\frac{1}{M} = \frac{\phi}{K_L} + \frac{b - \phi}{K_s} \dots\dots\dots (6)$$

where ϕ is porosity and K_L is the bulk modulus of the pore fluid. The reduced time is $\theta = t / \tau_v$ and the hydrodynamic relaxation time, τ_v is given by

$$\tau_v = \frac{\eta L R^2}{k} \left(\frac{\beta b^2}{K_p} + \frac{\phi}{K_L} + \frac{b - \phi}{K_s} \right) \dots\dots\dots (7)$$

where R is the cylinder radius, k is the permeability, and ηL is the viscosity of the pore fluid. An approximate equation for the relaxation function is given by

$$\Omega(\theta) \approx \exp \left\{ \frac{4}{\sqrt{\pi}} [1 - b\lambda(1 - \beta)] \left(\frac{\theta^{2.2} - \theta^{1/2}}{1 - \theta^{0.55}} \right) \right\} \dots\dots\dots (8)$$

The cylindrical sample is assumed to be long compared to its radius so that axial flow is minimal. The axial strain as a function of the reduced time is

$$\varepsilon_z = \varepsilon_\infty + (\varepsilon_\infty - \varepsilon_0) \Omega(\theta) \dots\dots\dots (9)$$

By fitting the measured axial strain to Equation (9) and determining the relaxation time, τ_v , the permeability may be determined from Equation (7).

6.3 Application of DP Test to Pervious Concrete

The particles of aggregate are connected with thin paste layer in pervious concrete such that flow of fluid accesses the coated aggregates from virtually all directions (see Figure 45). Therefore, while the analysis for a cylindrical geometry is appropriate for normal concrete cylinders, the analysis for pervious concrete requires a roughly spherical geometry. It is assumed in this analysis that the macropores which give pervious concrete its distinction are pressurized immediately upon the pressurization of the outer surface of the cylinder. Therefore, the start of the test effectively involves paste-coated aggregates surrounded by pressurized fluid.

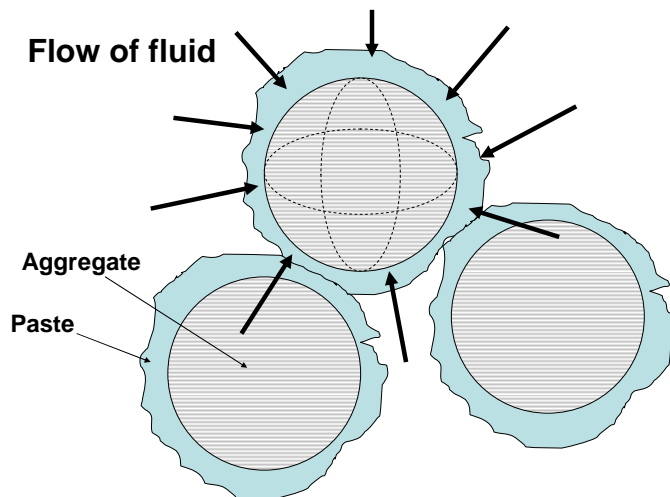


Figure 45 Illustration how pervious concrete is considered as a sphere model for the DP test.

When a spherically shaped sample is pressurized rather than a cylinder, the axial strain is still given by

$$\varepsilon_{\theta} = \varepsilon_{\infty} + (\varepsilon_0 - \varepsilon_{\infty})\Omega(\theta), \dots\dots\dots (10)$$

but according to Scherer (2006) the relaxation function is now given by

$$\Omega_s(\theta) \approx \exp \left\{ \frac{6}{\sqrt{\pi}} [1 - b\lambda(1 - \beta)] \left(\frac{\theta^2 - \theta^{1/2}}{1 - \theta^{0.5}} \right) \right\} \dots\dots\dots (11)$$

Figure 46 shows the relaxation functions for both the cylinder and sphere samples in terms of reduced time. For the pervious concrete, the measured axial displacement is considered to arise out of the cumulative displacement in the paste-coated aggregates along any vertical path through the cylinder. The rate at which the re-expansion occurs (represented by the relaxation function) is assumed to be dependent on the rate at which fluid flows into and pressurizes the paste coated aggregates. Because the paste layers are being pressurized first, followed by the aggregates within, one would expect to see at least two distinct relaxation curves in the measured axial data as a function of time. As we are primarily interested in the durability of the paste layer surrounding the aggregates, it is necessary that we know the thickness of that layer to correlate to the total distance of fluid travel (approximately equivalent to R in Equation (7)).

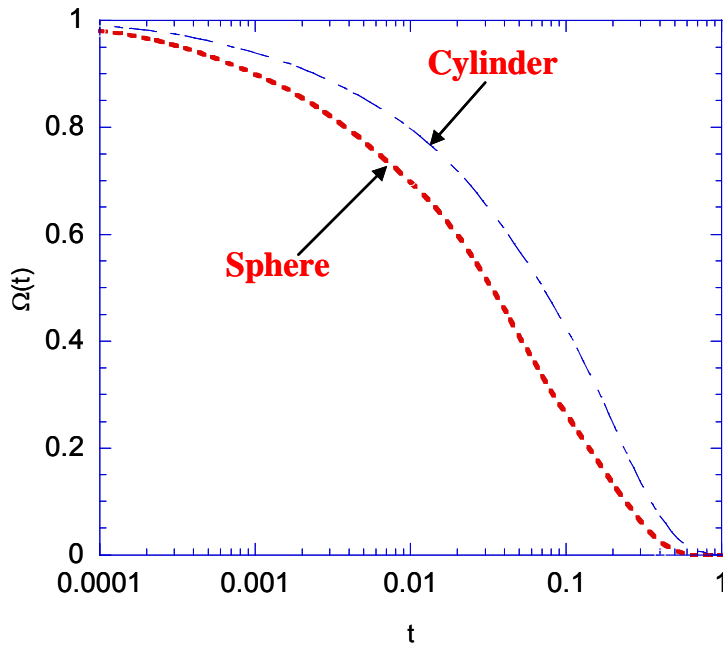


Figure 46 Comparison of cylinder and sphere relaxation functions, after Scherer (2006).

The thickness of the paste layer can be initially calculated using the initial mixture design in conjunction with the properties of the constituent materials. The volume of aggregates per unit volume of concrete (V_a) can be determined according to

$$V_a = \frac{M_a}{SG_a} \dots\dots\dots (12)$$

where M_a is the total mass of aggregate per unit volume of concrete and SG_a is the specific gravity of the aggregate.

We approximate each aggregate and paste coating as spherical as shown in Figure 47.

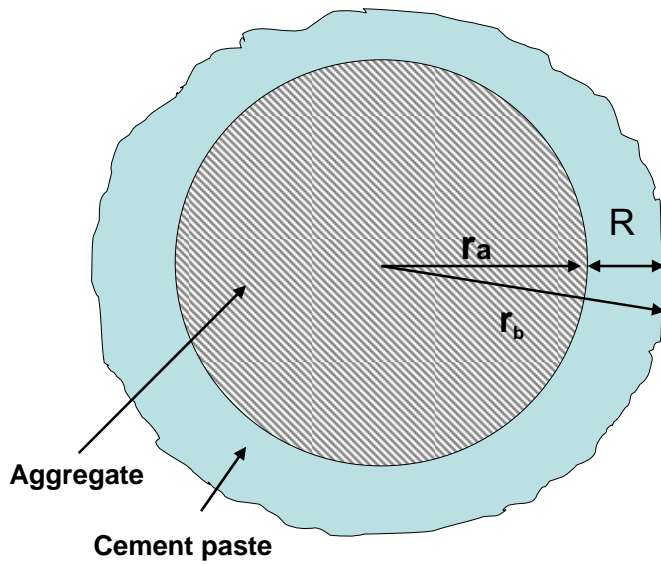


Figure 47 Illustration of an aggregate covered with cement paste. (r_a = radius of aggregate, r_b = radius of aggregate + paste, R = layer thickness of paste).

To calculate the volume of cement paste per aggregate particle (v_p), we need the ratio of total volume of paste to total volume of aggregate (V_a) as

$$v_p = \frac{\frac{M_c}{3.15} + \frac{M_w}{1}}{V_a} \dots\dots\dots (13)$$

where M_c is the mass of cement and M_w is the mass of water per unit volume of concrete in the mixture design.

The obtained v_p can be related to r_a , r_b , and R given by

$$v_p = \frac{4}{3} \pi r_b^3 - \frac{4}{3} \pi r_a^3 = \frac{4}{3} \pi (r_b^3 - r_a^3) \dots\dots\dots (14)$$

Then, Equation (14) may be rewritten as

$$r_b = \left[\left(\frac{3v_p}{4\pi} \right) + r_a^3 \right]^{\frac{1}{3}} \dots\dots\dots (15)$$

The thickness of paste layer can be calculated by

$$R = r_b - r_a \dots\dots\dots (16)$$

Table 5 lists the calculated layer thickness of paste for those specimens evaluated in the DP test. Each material tested is about 180 day old. Mixtures B and C are identical except that mixture C includes a high-range water reducer (HRWR).

Table 5 Paste layer thickness and mixture design parameters necessary for the calculation of the thickness.

| Mix number | A | B | C (B+HRWR) |
|--|----------|-----------|------------|
| Coarse aggregate (kg/m ³) | 1564.6 | 1227 | 1227 |
| Fine aggregate (kg/m ³) | 0 | 99 | 99 |
| Cement (kg/m ³) | 189.5 | 107 | 107 |
| Silica fume (kg/m ³) | 0 | 17.9 | 17.9 |
| Water (kg/m ³) | 56.1 | 107 | 107 |
| Air content (%) | 23 | 23 | 23 |
| Paste layer thickness | 0.4 (mm) | 0.55 (mm) | 0.55 (mm) |

6.4 Experimental Apparatus and Procedure

The specimen geometry for the DP experiment was a 4 in. x 8 in. (diameter x height) cylinder of pervious concrete. The mixing procedure of the pervious concrete for the DP test was the same as described in section 3.3. Specimens were demolded at an age of 12

hr and then stored in deionized water with a lime addition of 0.2 % to prevent leaching. Specimens were maintained in the limewater until the test initiation. A steel plate was epoxied to each end of the cylindrical specimen in order to attach the stainless steel measurement rod into the sample (for axial displacement).

At the start of the DP test, the concrete cylinder was placed in a sealed pressure chamber which was filled with lime water and oil up to the top of the chamber (see Figure 48). Axial displacement was measured with an LVDT, the core of which was attached to the end of the stainless steel measurement rod. When the electric hydraulic pump was turned on, the hydrostatic pressure was applied to the sample such that it contracted suddenly. The applied pressure was maintained constant throughout the test.

Since the pore pressure was less than the applied pressure, the fluid flowed into the pores and increased the pore pressure to the applied pressure; this caused the specimen to gradually re-expand as the pressure increased within the pore network (see Figure 49) Using a pressure sensor and LVDT, the pressure and axial displacement were measured as a function of time.

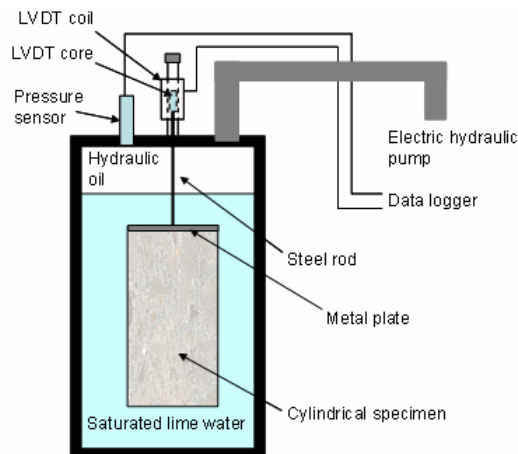


Figure 48 Apparatus for dynamic pressurization experiment, after Grasley (2006).

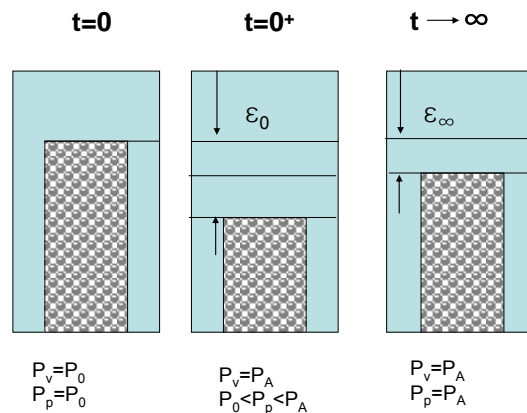


Figure 49 Illustration of dynamic pressurization experiment. The sample is placed in the vessel. The pressure in the vessel (P_v), the pore fluid (P_p), and atmospheric pressure (P_0) are equal. After starting the test ($t=0^+$), P_v increases up to some higher value (P_A). Simultaneously, the sample contracts by the changed pressure. The fluid gradually flows through the sample such that the pore pressure eventually reaches P_A . At long times, the final strain (ϵ_∞) is constant as the pore fluid pressure reaches P_A , after Scherer (2006).

6.5 Initial Trials and Results

The permeability of the paste coatings in pervious concrete, as determined from the DP test, requires several material properties of the pervious concrete and the pore solution including K_L , η_L , K_p , K_s , ν_p (Poisson's ratio of the porous body), and ϕ (porosity). The cement paste layer thickness R and the retardation time τ_v are also necessary properties for determining the permeability, k . The fluid properties (η_L , K_L) can be determined when the temperature and fluid are known. In this study, ν_p and K_p were approximated since these values do not strongly influence the calculated permeability, k . The parameter ν_p was estimated as 0.2 in this study. The porosity, ϕ , was obtained by

$$\phi = \left(1 - \frac{K_p}{K_s}\right)^{1/3} \dots\dots\dots (17)$$

(Vadakan and Scherer, 2002). K_s was approximated as 45 GPa based on previously measured values (Grasley et al., 2006). K_p was approximated based on a reasonable Young's modulus and Poisson ratio for the cement paste fraction of the concrete.

Figure 50 plots the typical measured axial strain response of pervious concrete in the DP test after being exposed to a step hydrostatic pressure of 1000 psi. The rate of re-expansion after pressurization slowly decreases until the strain levels off, indicated by point A on the Figure. The specimen once again begins to re-expand after point A, which is assumed to be due to the penetration of the fluid into the aggregates. Since the aggregates are covered with a rather thin paste layer (0.4~0.6mm) in this study, the long

test duration should be sufficient for fluid to infiltrate into the aggregate. It is also possible that the aggregates and their paste layers were not fully saturated. When the material is not fully saturated, fluid is forced into the pore network by the externally applied hydrostatic pressure, but the specimen does not re-expand as rapidly. This is because the entrapped air bubbles are easily compressed and therefore do not exert a swelling pressure on the surrounding solid material.

The w/c (0.3) in all the specimens in this study are relatively low, and may be difficult to fully saturate. It may be particularly difficult to saturate the aggregates which are coated with cement paste, and it may be prudent in future studies to pre-saturate the aggregates (SSD state) prior to mixing in order to make the results of the DP test more predictable.

In order to analyze the permeability of the paste layers coating the aggregates, only the first relaxation (before Point A) was analyzed since it is the hypothesis that this expansion is due to pressurization of the paste layer. Therefore, the following plots (Figure 51, Figure 52) showing the deformation response only show the initial re-expansion data prior to the first leveling-off of axial strain data.

Figure 51 shows the relaxation function of mixture A fitted to Equation (11). Based on this relaxation curve, the permeability, k , is $2.14 \times 10^{-24} m^2$. Previous research (El-Dieb and Hooton, 1995) has indicated that for low w/c materials such as used in this study the permeability should be roughly $1.86 \times 10^{-23} m^2 \sim 1.92 \times 10^{-23} m^2$, which is one order of magnitude higher than that obtained in this study for the pervious concrete paste layers using the DP test.

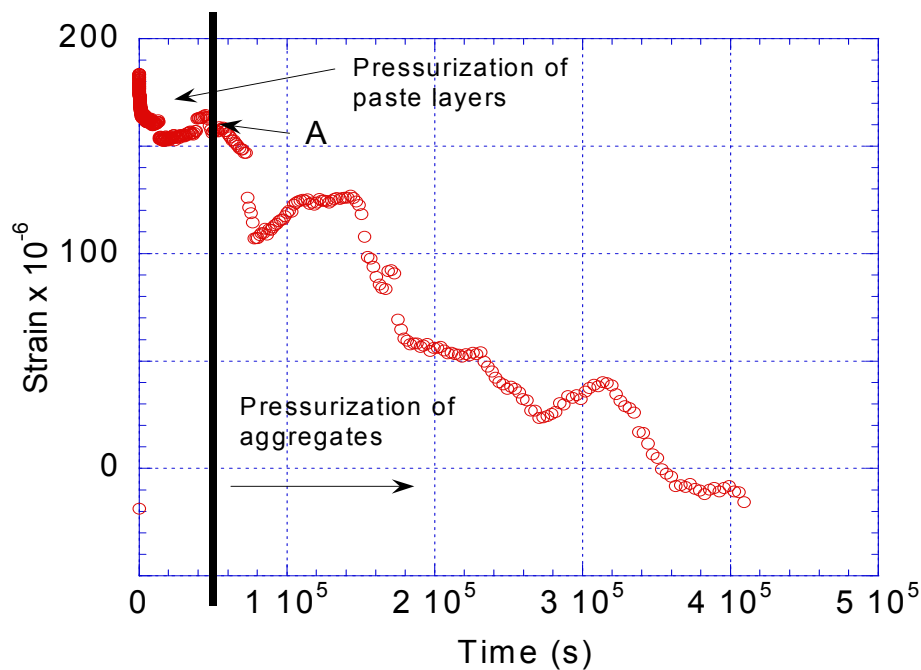


Figure 50 Typical long term response of pervious concrete to dynamic pressurization. Paste layer is influenced first, followed by pressurization of the aggregates. Entrapped air may affect inflection of point A.

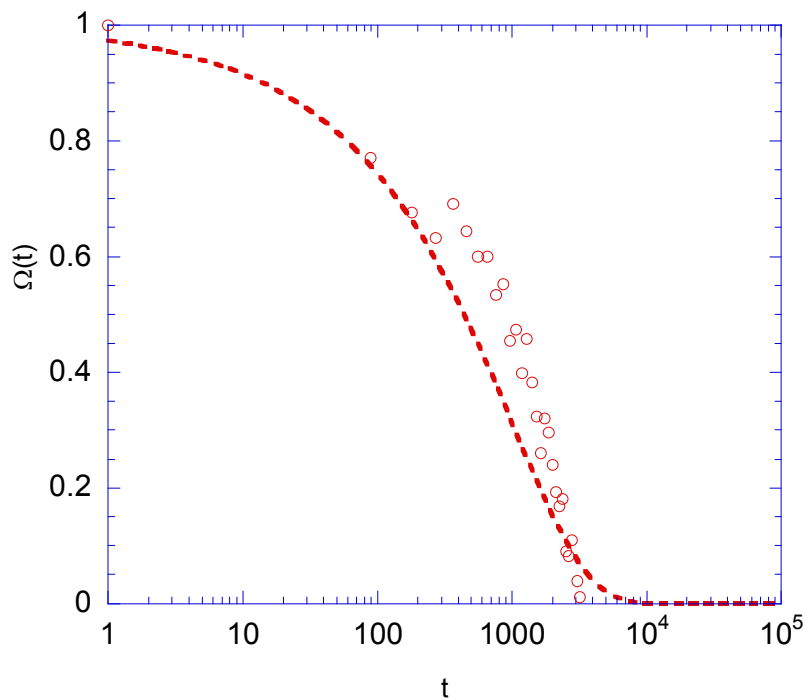


Figure 51 $\Omega(t)$ versus t on mixture A.

Figure 52 shows the relaxation function of mixture B. The permeability, k , of mixture B was calculated as $3 \times 10^{-25} m^2$, and k of mixture C was calculated as $7 \times 10^{-25} m^2$ (see Figure 53). El-Dieb and Hooton (1995) reported k of mixtures incorporating silica fume and HRWR as ranging from $1.93 \times 10^{-23} m^2$ to $2.14 \times 10^{-23} m^2$. The results from this study indicate a permeability that is two orders of magnitude lower than obtained by El-Dieb and Hooton (1995). Moreover, the permeabilities of mixture C and D are less than A such that the usage of silica fume and HRWR reduce permeability of the paste layer.

There are a few possible explanations for the poor agreement between the measured permeabilities of the paste layers coating the aggregates as determined in this study and the permeability values reported for normal concrete materials with similar w/c. First,

there could have been entrapped air bubbles in the DP experiments. The presence of entrapped air would delay the re-expansion behavior and would also help explain the poor fit of the measured data to the relaxation function. Second, the literature values could be overestimates of the real material permeability owing to leaks. It is very difficult to obtain an accurate flow-through permeability measurement on such low permeability materials. In any event, more research is necessary to fully understand the results from the DP measurement on pervious concrete and to develop confidence in the calculated permeability of the cement paste layers coating the aggregates.

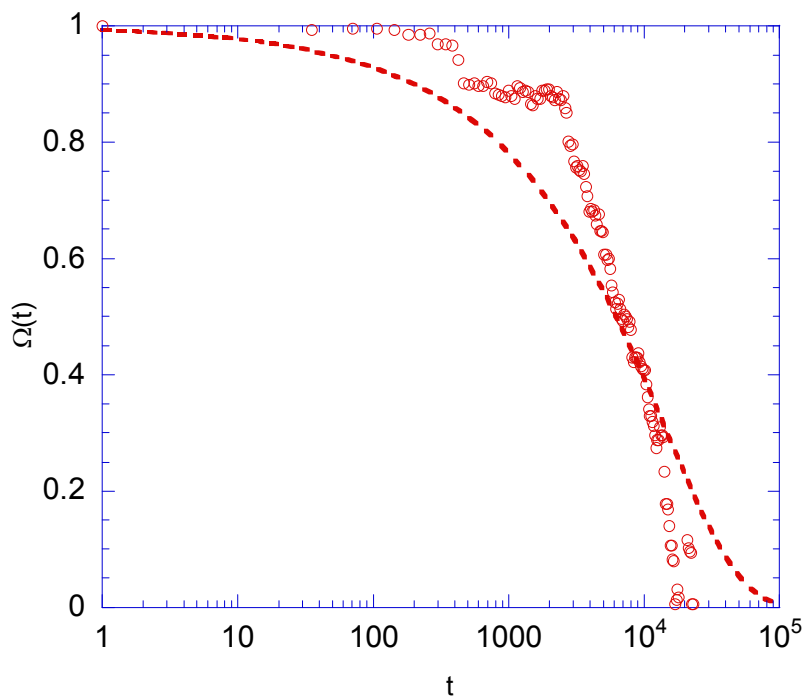


Figure 52 $\Omega(t)$ versus t on mixture B.

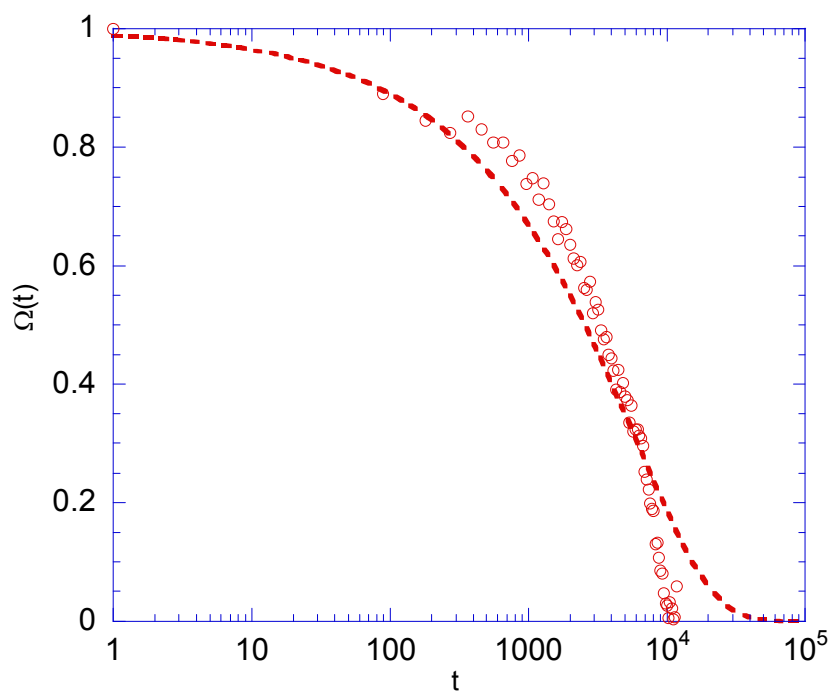


Figure 53 $\Omega(t)$ versus t on mixture C.

7 SUCTION MODEL

7.1 Motivation

Clogging is a problem for pervious concrete pavement due to debris and dirt that fill the pore network such that pervious concrete does not drain properly. Maintenance of pervious concrete is often performed to prevent clogging of the pore structure of the surface of pervious concrete. The ACI committee report briefly introduces three methods to clean pavement surface such as vacuuming, power blowing, and pressure washing (Tennis et al., 2004). These methods need cost to maintain pavement surface properly.

A self-cleaning effect on pervious concrete pavement may occur without maintenance during heavy rainfall. To be specific, it has been noted that vehicle speed and hydraulic action of vehicle tires affect the clogging materials in pervious asphalt during heavy rainfall. When suction of water takes place at the edge of tire, the clogging particle in pervious concrete may be removed by a pressure gradient, which is referred to as a self-cleansing effect (Sandberg, 1999; Varadhan, 2004). This study will involve the investigation of the effect of passing vehicle tires on clogged particles in pervious concrete.

The objective of this section is to develop a simple model for predicting removal of clogging particles from pervious concrete pavement surface pores through suction induced by vehicle tires passing over the clogged pore. The motivation is to develop a

tool to be used for designing the surface layer of pervious pavement that is resistant to permanent clogging.

7.2 Suction Model Introduction and Assumption

Figure 54 shows a vehicle wheel passing over a pervious concrete pavement with water present. Modeling suction is quite complex because hydroplaning is generated by moving wheel. This problem has not been investigated in the current literature. A simple geometric model will be derived from the interaction of the vehicle tire and the pore in the following section.

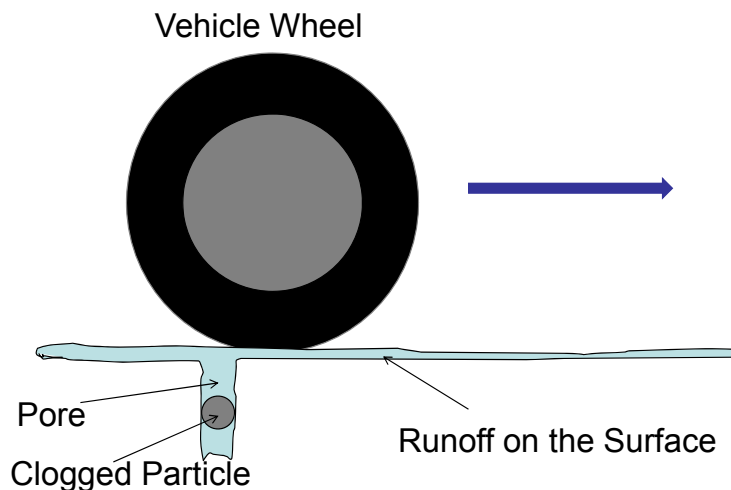


Figure 54 Illustration of clogged pore in pervious concrete pavement while the vehicle wheel is passing over.

Figure 55 describes how a particle moves upward as a result of a moving vehicle tire. When the vehicle tire passes over a pore in pavement surface, pressure on pore structure of pervious concrete pavement changes due to water volume change. This volume

change is induced by a certain adhesion force between tire rubber and water on surface stretching the water as the tire passes over the pore. Mean fluid velocity is approximated by using Hagen-Poiseuille equation. In addition, the pressure gradient between the vehicle tire and pavement surface causes fluid flow to occur in the pores of pervious concrete pavement. Kutay (2007) measured the positive (compressive) pressure gradient at the surface of pavement specimens under both steady and dynamic pressures caused by the downward force applied by the vehicle tire. Based on Kutay's results, this pressure gradient is extremely small compared with the negative (tensile) suction pressure such that it is not counted in this study. Since the frictional shear stress in the pore fluid, τ_c , is also fairly small, it is not considered in this model. The downward force, such as gravity, is calculated using Stokes' Law.

In brief, the particle position can be approximately derived by taking into account equations such as Hagen-Poiseuille Law and Stokes' Law. The equation for the particle vertical position is simply determined as

$$Y_{particle\ position} = Y_{fluid} - Y_{sink} \dots\dots\dots (18)$$

where, Y_{fluid} is the vertical position of the center of volume of the fluid within the pore as a result of Hagen-Poiseuille Law, and Y_{sink} is the vertical distance by which the particle sinks within the fluid as a result of Stokes' Law.

Then, several factors such as tire radius, vehicle velocity, tire position, pore radius, and depth of pore are used to determine the parameters in equation (18) in the following section. It is assumed that the radius of the particle is equal to the radius of pore to minimize unknown values.

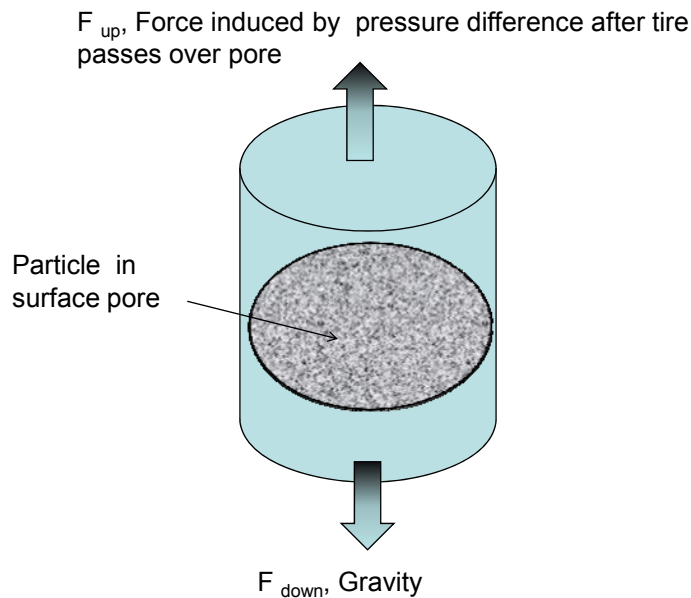


Figure 55 Illustration of upward and downward force, which influence position of particle in pore structure.

7.3 Suction Model Assumptions and Derived Equations for $Y_{particle}$

Analytical functions for the suction of a particle out of a cylindrical surface pore in pervious concrete are derived in the following equations. This involves the determination of the particle vertical position ($Y_{particle}$) as a function of tire horizontal position with respect to the tire radius, vehicle velocity, tire position, pore radius, and depth of pore, etc. Moreover, the pressure as a function of X (horizontal distance from

center of tire to the center of pore) can be determined to evaluate X_{\max} , which is the distance when water becomes detached between vehicle tire and pavement surface. The vertical position of the tire, Y_{tire} is a geometrical function of only X and the tire radius, R based on geometry. We can write

$$\theta = \text{Arc sin}\left(\frac{S}{R}\right), \dots\dots\dots (19)$$

where S is half of \overline{bc} , and R is tire radius, and θ is $\angle bac$ (see Figure 56).

In addition,

$$\text{Tan}(\theta) = \frac{Y_{tire}}{X}, \dots\dots\dots (20)$$

where Y_{tire} is the distance from the tire to the pavement surface at distance X . From the Pythagorean theorem,

$$X^2 + Y^2 = 4S^2 \dots\dots\dots (21)$$

Solving the three equations above for Y_{tire} as a function of X and R results in

$$Y_{tire} = R - \sqrt{R^2 - X^2} \dots\dots\dots (22)$$

Equation (22) is derived from the assumption that the bottom of the tire is not in planar contact with the pavement. Instead, the bottom spot of tire is contacted at the point of c (see Figure 56). In reality, the bottom spot of tire contacted on pavement is not a point

but a certain configuration such as a rectangle and two semicircular ends (Huang, 2004).

Equation (23) is derived by accounting for the correct contact configuration such that

$$Y_{tire} = \frac{1}{2}(\sqrt{-contact\ length^2 + 4R^2} - 2\sqrt{R^2 - X^2}) \dots\dots\dots (23)$$

The resulting model is not substantially influenced by tire contact configuration as determined from evaluating the model results using both Equations (22) and (23).

Therefore, equation (22) is utilized from this point on since it is simpler.

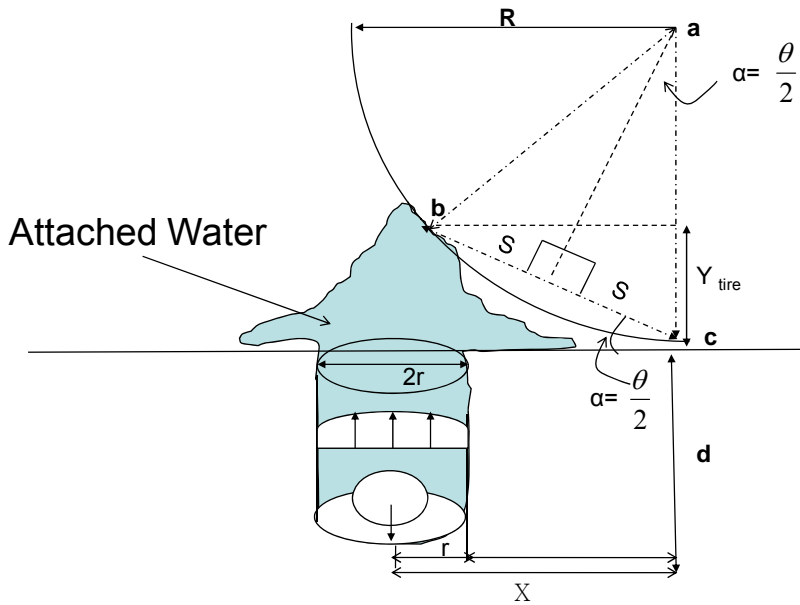


Figure 56 Geometry between tire and pore in pavement surface is described.

Figure 56 illustrates the full suction problem geometry where R is radius of vehicle tire, r is radius of a cylindrical pore, d is depth of a cylindrical pore, X is the horizontal distance from bottom of tire to the center of the pore, Y_{tire} is the vertical distance

between the pavement surface and the tire surface at a horizontal distance X . The parameter θ is $\angle bac$, and S is half of \overline{bc} .

Y_{fluid} can be determined by integrating the velocity of the fluid (v_f) as determined by Hagen-Poiseuille's equation, which is

$$v_f \pi r^2 = \frac{\pi r^4}{8\eta} \frac{|\Delta P|}{d} \dots\dots\dots (24)$$

where, v_f is mean fluid velocity along the length of the cylindrical pore (m/s), r is radius of the cylindrical pore (m), ΔP is pressure difference between the two ends (Pa), η is dynamic fluid viscosity ($Pa \cdot s$), and d is depth of the cylindrical pore (m)

Equation (24) can be expressed in terms of v_f as

$$v_f = \frac{r^2}{8\eta} \frac{|\Delta P|}{d} \dots\dots\dots (25)$$

When a friction factor (f) to account for non-laminar conditions is added into the above equation, Equation (26) can be expressed as

$$v_f = f \frac{r^2}{8\eta} \frac{|\Delta P|}{d} \dots\dots\dots (26)$$

The original water volume of the cylindrical pore is $\pi r^2 d (m^3)$ (see Figure 57). After vehicle tire passes over the pore, the small amount of water is bonded to tire surface by the adhesive strength between tire rubber and water. Then, the water volume of pore

structure is changed to $\pi r^2 [Y_{tire} + (d - Y_{fluid})]$ (m^3). It is assumed that the volume of water is not effected by excessive water on the pavement surface filling the pore during the suction problem. Therefore,

$$\begin{aligned}
 Y_{diff} = \Delta d &= \text{changed depth of pore} - \text{original depth of pore} = [Y_{tire} + (d - Y_{fluid})] - d \\
 &= Y_{tire} - Y_{fluid}
 \end{aligned}
 \dots\dots\dots(27)$$

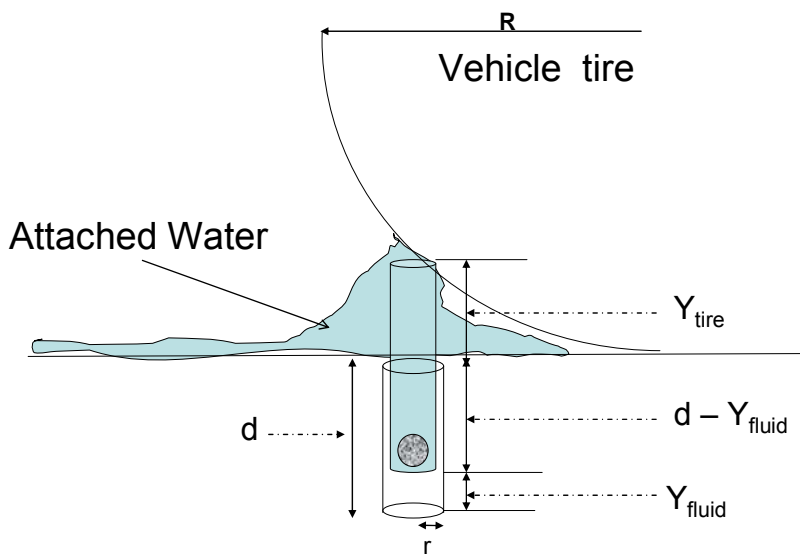


Figure 57 Geometry explaining how volume of water in pore structure is changed when vehicle tire passes over.

Strain of water volume can be expressed as

$$\varepsilon = \frac{\Delta V}{V} = \frac{\pi r^2 Y_{diff}}{\pi r^2 d} = \frac{Y_{diff}}{d} \dots\dots\dots(28)$$

in addition, bulk modulus can be simply expressed as

$$K_L = \frac{\Delta P}{\varepsilon}, \dots\dots\dots (29)$$

where K_L is the bulk modulus of fluid. To determine ΔP , solving above Equations results in

$$\Delta P = \frac{Y_{diff}}{d} K_L \dots\dots\dots (30)$$

From Equation (26), the only unknown value is ΔP , which was determined in Equation (30) Thus, v_f can be expressed in terms of K_L , Y_{diff} , which is

$$v_f = f \frac{r^2}{8\eta} \frac{K_L Y_{diff}}{d^2} \dots\dots\dots (31)$$

v_f can be expressed using V_h , vehicle horizontal velocity, and Y_{fluid} based on a geometrical function. Fluid velocity can be calculated in terms of moved distance of fluid and time. It is simply

$$v_f = \frac{dY_{fluid}}{dt} \dots\dots\dots (32)$$

In addition, vehicle speed can be expressed in terms of moved distance of vehicle and time, which is

$$V_h = \frac{dX}{dt}, \dots\dots\dots (33)$$

where dt is involved in above equations such that v_f can be solved as

$$v_f = \frac{dY_{fluid}}{dX} V_h \dots\dots\dots (34)$$

Through Hagen-Poiseuille's equation, fluid velocity can be determined by internal pore structure factors such as r , d , and Y_{diff} . Fluid velocity is also solved by external factors such as V_h and X . Thus, Y_{fluid} can be determined by substitution of equations (31) and (34) such that Y_{fluid} can be expressed in terms of internal and external factors as

$$f \frac{r^2}{8\eta} \frac{K_L Y_{diff}}{d^2} = \frac{dY_{fluid}}{dX} V_h \dots\dots\dots (35)$$

Both sides of the above equation include Y_{fluid} . Equation (35) may be solved to obtain

$$Y_{fluid} = \int_0^x \frac{fr^2 K_L Y_{diff}}{8d^2 \eta V_h} dX \dots\dots\dots (36)$$

Through substitution of previously defined variables, one obtains

$$Y_{fluid} = - \frac{fr^2 \left[X \left(-2R + \sqrt{R^2 - X^2} \right) + R^2 \text{ArcTan} \left(\frac{X}{\sqrt{R^2 - X^2}} \right) \right] K_L}{2 \left(8d^2 V_h \eta + fr^2 X K_L \right)} \dots\dots\dots (37)$$

Y_{sink} is initially derived by using Stokes' Law. Then, the result from Stokes' Law is calculated in the same procedure of Equation (32), and (33). Here, Y_{sink} is

$$Y_{\text{sink}} = \frac{2gr^2 X(\rho_p - \rho_f)}{9V_h \eta} \dots\dots\dots (38)$$

where, g is gravitational acceleration (m/s^2), ρ_p is density of particle (kg/m^3), ρ_f is density of fluid (kg/m^3), and all other variables are as previously defined.

Up to now, both Y_{fluid} and Y_{sink} are determined to solve the vertical position of particle in pore. Before approaching the final answer, it is necessary to assume that particle is sucked out when water moves up. It means that the particle movement of water in pore plays an important key in controlling suction of particle. Combining Equations (18), (37), and (38), the final equation for the vertical position of the particle is obtained as

$$Y_{\text{particle}} = \frac{1}{18} r^2 \left\{ - \frac{9f \left[X(-2R + \sqrt{R^2 - X^2}) + R^2 \text{ArcTan} \left(\frac{X}{\sqrt{R^2 - X^2}} \right) \right] K_L}{8d^2 V_h \eta + fr^2 X K_L} + \frac{4gX(\rho_f - \rho_p)}{V_h \eta} \right\} \dots\dots\dots (39)$$

7.4 Evaluation of Maximum Distance, X_{max}

The attached water between vehicle tire and surface pavement would rupture when vehicle moves forward within certain distance, X . The assumption is based on surface energy, which may mostly affect bond strength between tire rubber and water. Thus, it is assumed that the maximum distance X that the center of the tire can be from the center

of the radius of the cylindrical pore is determined by the maximum negative suction pressure (see Figure 56). In this study, the adhesive failure pressure is necessary to determine P_{\max} between tire rubber and water in pore. P_{\max} can be determined by using Equilibrium theory of adhesion between a cylinder and a plane (Kendall, 1971). The Equation is

$$P_{\max} = \sqrt{\frac{8\pi}{(1-\nu)^2} \frac{E\gamma_{rw}r^3}{\pi r^2}} \dots\dots\dots (40)$$

where, E is Young's modulus of the rubber, ν is the Poisson's ratio of the rubber, r is the radius of the cylinder of water adhered to the rubber tire, γ_{rw} is the surface energy between rubber and water.

According to Agrawal (2008), Young's modulus of rubber is $6 \times 10^6 Pa$. The Poisson's ratio of rubber is assumed to be 0.49 in this study. The only unknown value, γ_{rw} , can be determined by using Young's Equation which is

$$\gamma_{ar} = \gamma_{rw} + \gamma_{aw} \cos \theta \dots\dots\dots (41)$$

where, γ_{ar} is the surface tension of rubber in air, γ_{rw} is the surface tension of rubber and water interface, γ_{aw} is the surface tension of water in air, θ is the contact angle measured from between water and rubber.

Typically, contact angle ranges from 90 to 103 degree such that contact angle was used 90 degree as minimum value in this study. Approximated values of γ_{aw} , γ_{ar} are respectively 0.072, 5, which result in γ_{rw} as 4.996 in this study. After substituting γ_{rw} into Equation (40), P_{max} is determined in terms of radius of pore structure, r . Therefore, P_{max} is

$$P_{max} = \frac{17236.5\sqrt{r^3}}{r^2} \dots\dots\dots (42)$$

Figure 58 shows the relationship between radius of pore and P_{max} . As r approaches zero, P_{max} increases. X_{max} , maximum distance from the bottom of vehicle tire to the pore, can be determined through $Y_{diff-max}$.

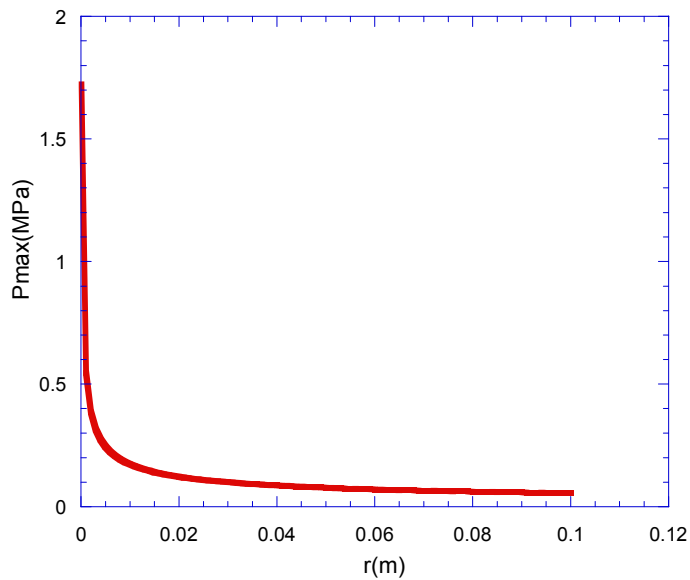


Figure 58 radius of pore structure vs P_{max} .

Equation (30) can be rewritten as

$$Y_{diff-max} = \frac{P_{max} d}{K_L} \dots\dots\dots (43)$$

Here, P_{max} is approximated as either 150×10^6 MPa (for cohesive rupture within the water), or is determined based on Equation (42) for adhesive rupture. For example, for cohesive rupture,

$$Y_{diff-max} = \frac{150 \times 10^6 d}{K_L} \dots\dots\dots (44)$$

From Equation (27), Y_{diff} can be determined by using known values such as Y_{lire} from Equation (22) and Y_{fluid} from Equation (37). In addition, the failure will be adhesive for all practical pore sizes. Thus, when Equation (44) is set equal to Equation (27) to determine X_{max} ,

$$Y_{diff-max} = \frac{150 \times 10^6 d}{K_L} \\ = R - \sqrt{R^2 - X^2} + \frac{fr^2 \left[X \left(-2R + \sqrt{R^2 - X^2} \right) + R^2 \text{ArcTan} \left(\frac{X}{\sqrt{R^2 - X^2}} \right) \right] K_L}{2(8d^2 V_h \eta + fr^2 X K_L)} \dots\dots (45)$$

Since X_{max} can not be solved analytically in the above equation, practical values such as Table 6 are applied for Equation (45).

Table 6 Input values for equation (45).

| Input data | values |
|--|-------------------|
| f , coefficient of friction | 1 |
| Vh , vehicle speed (m/sec) | 35 |
| ρ_p , density of particle (kg/m^3) | 2650 |
| ρ_f , density of fluid (kg/m^3) | 1000 |
| g , gravity (m/sec^2) | 9.81 |
| r , pore radius (m) | 0.001 |
| R , vehicle radius (m) | 0.2 |
| η , viscosity of fluid ($Pa \cdot sec$) | 0.00089 |
| K_L , bulk modulus of liquid (kg/m^2) | 2.2×10^9 |
| d , depth of pore (m) | 0.001 |

X_{max} is a function of various values such that above input values were assumed to approximate proper X_{max} . In conclusion, it may be expected to obtain reasonable X_{max} for suction model. The result, however, is considerably small distance such as around $0.006m$ such that suction may be allowable to occur only immediately after the tire passes before the water detaches from the tire due to adhesive failure. Since this model is developed mostly based on adhesive bond strength between tire surface and water inside pore, suction would not take place beyond the failure of adhesive bond strength.

The value of X_{max} determined in this model directly results from the failure of adhesive strength such that suction only occurs within X_{max} (before the water detaches from the

tire rubber). The extremely small value determined for X_{\max} is probably not realistic, and is therefore a crude approximation in this model.

7.5 Evaluation of the Vertical Position of Particle

The vertical position of particle can be calculated using Equation (39). According to the following figures such as Figure 59, Figure 60, and Figure 61, the vertical position of particle is shown versus X as changing input values. It is determined that X should be longer than 0.04 (m) by using Table 6 if suction occurs in this model. According to previous tasks, X_{\max} was determined less than 0.04 (m). Therefore, this suction model is not appropriately allowable to predict suction problem in pervious concrete pavement such that a certain theories which are related to more detailed hydraulic, and dynamic motion should be required to model suction phenomenon accurately.

Despite the limitations of the model derived in the preceding pages, the influence of various parameters on the ability of particles to be sucked out of pervious pavement is still able to be analyzed qualitatively if not quantitatively.

Figure 59 describes how vehicle speed affects vertical position of the clogging particle in a surface pore. As vehicle speed increases, the rate that pore fluid is sucked out of a surface pore increases relative to the rate at which the particle sinks in the fluid due to gravity. Low speeds such as 13 (m/s) does not cause the clogged particle to be sucked from the pore in pervious concrete pavements. On the other hand, the particle moves upward after vehicle tire passes over a certain horizontal distance under higher speeds

such as 25 and 35 (m/s). Therefore, higher vehicle velocity will increase the probability that particles can be sucked out of surface pores as a tire passes over the pore.

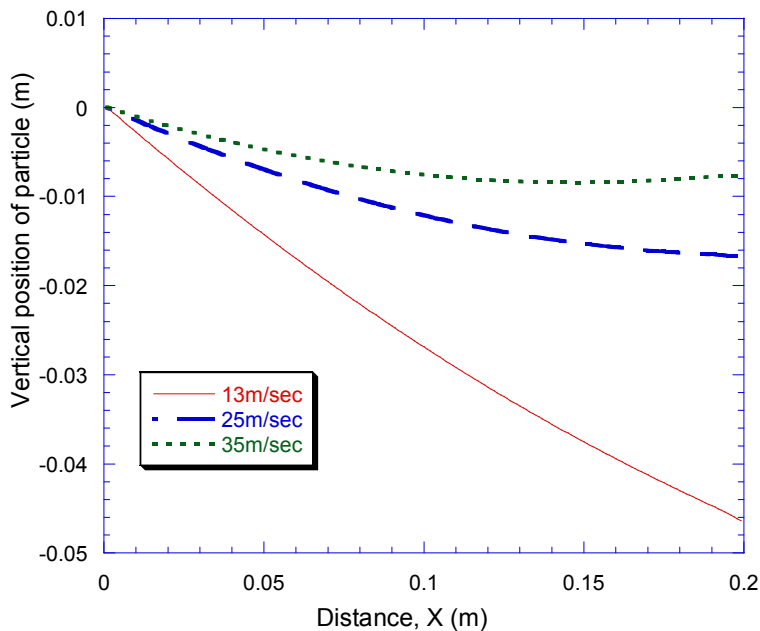


Figure 59 Relationship between horizontal distance and vertical position of particle in terms of various vehicle speed.

Figure 60 indicates how the vertical position of a particle is affected by the density of particles. As density of particle increases, the rate at which pore fluid is sucked out of a surface pore decreases relative to the rate at which the particle sinks in the fluid due to gravity. The results shows that the particle such as heavy sand, or metal debris would not be sucked out of pervious concrete pavement under vehicle speed, 35 (m/s). Instead, lighter materials such as light sand, rubber debris could move upwardly due to suction. Thus, lower density clogging particles have more potential to be removed when suction takes place.

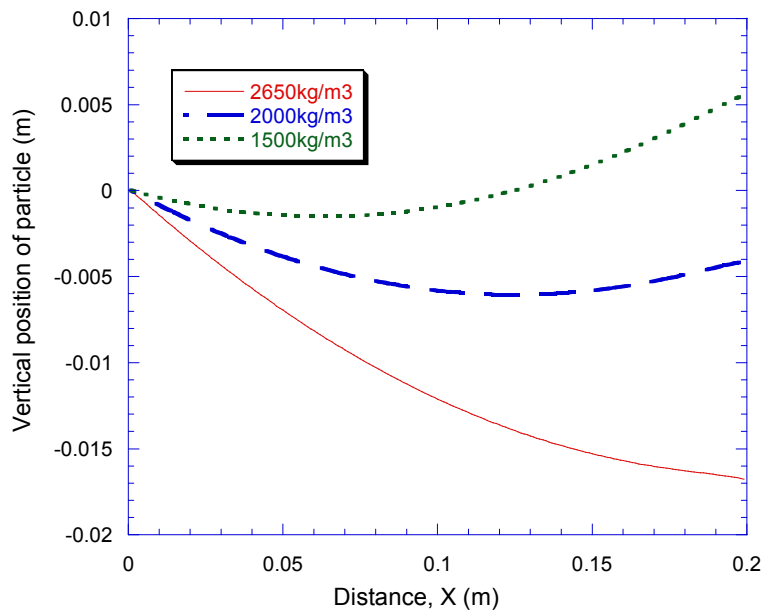


Figure 60 Relationship between horizontal distance and vertical position of particle in terms of various density of clogging materials.

Figure 61 shows the relationship between radius of pore and vertical position of particle. As radius of pore increases, the rate at which pore fluid is sucked out of a surface pore decreases relative to the rate at which the particle sinks in the fluid due to gravity. This result indicates that suction modeling in this study is more dependent upon radius of pore than other variables such as vehicle speed, density of particle. Radius of pore is likely to govern suction modeling since the vertical position of a particle is substantially varied with different radius of pore. Thus, minimizing pore size of upper surface pervious concrete pavement is helpful to not only prevent particle from being transferred into inside pavement, but also to remove clogged particle out of pore in pervious concrete pavement through tire suction.

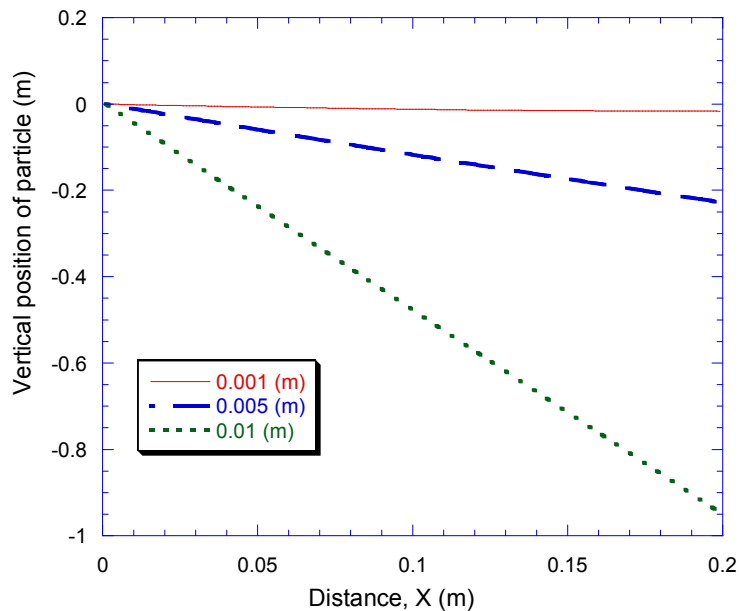


Figure 61 Relationship between horizontal distance and vertical position of particle in terms of surface pore radius pervious concrete.

Figure 62 shows the comparison between Y_{sink} , vertical position of particle induced by gravity, and Y_{fluid} , vertical position of particle induced by suction. Y_{sink} intends to affect the vertical position of particle to as decreasing linearly within some distance, then Y_{fluid} become higher than value of Y_{sink} as increasing gradually. Thus, Y_{sink} is determined to govern the vertical position of particle within X_{max} . Effectively, there is a competition between the rate at which pore fluid is sucked out of the pavement and the rate at which the particle sinks in the fluid. If the particle sinks faster than the fluid is sucked out, then the particle will remain in the pore.

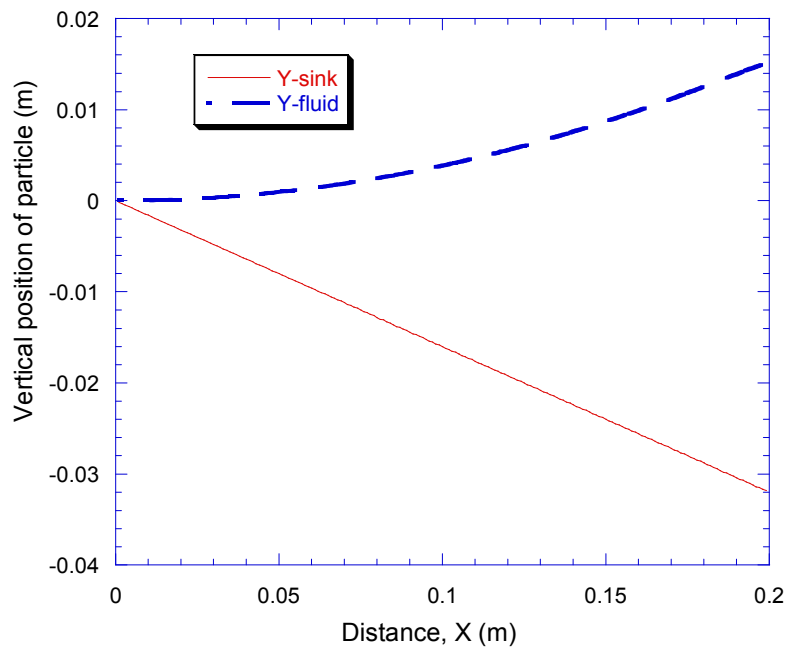


Figure 62 Relationship between horizontal distance and vertical position of particle

in terms of Y_{sink} and Y_{fluid} .

8 SUMMARY

The regulations of storm water management put forth by the U.S. Environmental Protection Agency (EPA) have elucidated a need for pavements that eliminate surface runoff. In general, conventional roadways are incapable of effectively managing stormwater runoff.

Pervious concrete can remove storm water more quickly than traditional concrete such that pervious concrete is a potential solution for eliminating stormwater runoff. In addition, pervious concrete has other advantages, including improving skid resistance and absorption of sound generated in the pavement. However, pervious concrete has several limitations preventing widespread application to normal roadways. The limitations of pervious concrete are related to strength, durability, and maintenance.

The study objectives were to:

- (a) Investigate the effect of mixture design (including the use of fibers) on the strength of pervious concrete
- (b) Evaluate effect of clogging materials on coefficient of permeability
- (c) Investigate dynamic pressurization test as a potential tool to evaluate durability of pervious concrete
- (d) develop a simple model for predicting removal of clogging particles from pervious concrete pavement surface pores

This thesis documents the influence of aggregate amount, aggregate size, different gradation of aggregate, cementitious materials, cement content, void ratio, unit weight,

and the use of fibers on compressive and flexural strength of pervious concrete. A typical pervious concrete mixture design was utilized as a control mixture. As a general finding, those changes in mixture design which increased the void ratio tended to reduce compressive and flexural strength while increasing permeability. The use of mineral admixtures had varying effects; the mixture utilizing class C fly ash exhibited a higher compressive and flexural strength, and high permeability. However, adding silica fume or silica fume with HRWR did not increase either compressive or flexural strength of pervious concrete; this apparently counter-intuitive result is caused by the 'patchy' coatings of cement paste on the aggregate particles when silica fume is used. Addition of fibers does not significantly increase flexural strength in comparison with control mixtures. Because of the rather thin layers of paste coating the aggregate particles, fibers did not anchor well and were easily pulled out. The mixtures containing higher cement paste resulted in higher compressive and flexural strength than other mixtures. However, mixtures with high paste content were still over-designed for flow rate; this is an important finding which implies that typical pervious concrete mixtures may be redesigned for higher strength while still meeting necessary permeability requirements.

The mixtures that had higher void ratios than 33% were not able to be clogged with sand in the clogging tests performed. These samples also had the highest coefficient of permeability among all tested samples. The permeability of mixtures having 24%, 25%, and 31% void ratios were substantially reduced through clogging by the sand. Though various void ratios existed in this group, permeability of these samples did not depend on air void ratio, but rather the size and connectivity of the specimen pore structure.

Therefore, to evaluate deterioration of permeability due to clogging, it is necessary to perform a clogging test rather than relying on void ratio to indicate probability of clogging.

In the clogging test, an average coefficient of permeability reduced from 0.36 to 0.29 (cm/sec) after the first clogging cycle. After adding clogging sand five times, an average coefficient of permeability decreased from 0.36 to 0.22 (cm/sec). The largest incremental decrease of permeability occurred after the first clogging cycle.

One objective of this study was to evaluate the ability of the DP test to quantify the durability of pervious concrete. The DP test is capable of measuring the permeability of nano-micro pore structure of the paste layers coating the aggregate particles rather than the flow-through permeability. The flow-through permeability of pervious concrete is purposely high; durability problems such as alkali-silica reaction and delayed ettringite formation will be controlled by the rate at which water/ions can penetrate into the small pores in the paste layers coating the aggregate particles.

The ability of the DP test to be used as a tool to evaluate pervious concrete durability is inconclusive from the results of this study. Complicated re-expansion behavior was measured which resulted from the sequential pressurization of the aggregates following the pressurization of the paste layers. An attempt was made to extract the re-expansion behavior associated strictly with the cement paste layer in order to quantify this value.

However, this was often difficult due to the complicated re-expansion data that exhibited multiple re-expansion curves in succession.

Based on the DP measurements, the permeability of pervious concrete (paste layers) is lower than conventional concrete. This is sensible since the w/c of the pervious concrete investigated in this study was very low (0.3). While this lower permeability would make the material more durable, the low thickness of the paste layers means that ions do not have far to travel to fully saturate the cement paste in pervious concrete.

The last objective of this study is to develop a simple model for predicting removal of clogging particles from pervious concrete pavement surface pores due to tire suction. It is noticed that vehicle speed influences suction of clogging materials in pervious pavement in literature. In this model, effect of vehicle speed is verified to affect suction of clogging materials in pervious concrete pavement. Vehicle speed is one of the sources to compensate the force of gravity ; as vehicle speed increases, the rate at vertically which pore fluid is sucked out of a surface pore increases relative to the rate at which the particle sinks in the fluid due to gravity.

Two sources of pressure gradient in this model were introduced such as adhesion force, and internal fluid pressure inside pore. The pressure gradient induced by internal fluid pressure would not affect movement of clogged particle due to comparably small pressure. In this study, pressure gradient induced by adhesion force can be evaluated to affect the clogged particle just after vehicle passes over pavement.

Pore size is one of the most significant factors to affect vertical position of particle. As size of pore increases, suction has less potential to occur in pervious concrete pavement. According to previous section, the use of smaller size of coarse aggregate is constructed to minimize that clogging material flows with rainfall into the inside pavement structure. In addition, the use of smaller size of upper surface pavement indicated that the clogged particle would be sucked out such that it intends to be helpful for self-cleaning effect.

9 RECOMMENDATION AND CONCLUSIONS

9.1 Recommendation on Mixture Proportioning

Concrete mixtures containing three different gradations of coarse aggregate were investigated in this study. Concrete mixtures containing the large, single-size coarse aggregate exhibited the lowest compressive and flexural strength, which was attributed to the reduced interconnectivity of the paste layers coating the aggregates when a uniform gradation was used.

According to the ACI 522 report on pervious concrete (2006), typical coarse aggregate size ranges from 9.5 to 19 mm. In this study, the concrete utilizing the small coarse aggregate size (9.5 mm) showed higher strength than the control mixture. The use of smaller size coarse aggregates reduces the void ratio and increases the interconnecting bonds between the paste layers resulting in a higher strength.

All concrete samples tested in this study had a w/c of 0.3. For the control mixture, the ratio of binder to aggregate (by mass) was approximately 0.27. The fresh pervious concrete was very stiff because of the low w/c and binder to aggregate ratio. Due to the stiff, unworkable nature of the pervious concrete, the utilization of silica fume led to a patchy paste coating on the aggregate particles and a reduced compressive strength. This is contrary to typical concrete where moderate additions of silica fume increases compressive strength. Both class C fly ash and higher cement contents resulted in higher

compressive and flexural strength. The use of fiber reinforcement did not improve the compressive or flexural strength of pervious concrete because the fibers were not well coated with paste and therefore were easily pulled out from the matrix. In general, it is anticipated that traditional straight fiber reinforcement will provide a minimal improvement in flexural strength and toughness for pervious concrete. Further research could investigate the ability of crimped, textured, or other fiber types/shapes to bond more efficiently in pervious concrete such that flexural strength and toughness are increased.

Based on measured permeability, the typical pervious concrete investigated in this study was over-designed for flow rate. It is recommended that the mixture proportions utilized in this research project be optimized by increasing paste content to increase strength since the materials are all over-designed for flow-rate. The ratio of binder to aggregate of 0.4 (by weight) resulted in the highest compressive and flexural strength. This mixture also had the lowest void ratio; however, this material (No.3-3) was more permeable than necessary for a 100-year extreme rainfall event (based on Austin, TX historical data). Therefore, reducing void ratio to improve strength should allow pervious concrete to overcome many of its structural deficiencies through increases in strength and durability while maintaining adequate permeability to handle 100-year rain events.

9.2 Conclusions

The limitations of pervious concrete, which are linked to strength, durability, and maintenance, have been investigated to evaluate and optimize pervious concrete for

application in urban areas. Typical pervious concrete is over designed for permeability based on extreme rainfall events; therefore, it is recommended to improve the material compressive and flexural strength at the expense of the permeability. By reducing the permeability of the pervious concrete in order to increase the strength, the clogging risk is increased. Based on the results of this study, clogging tends to reduce the permeability of materials with a void ratio less than 33%. Future research will investigate the possibility of designing pervious concrete materials with a void ratio less than 33% that are resistant to clogging.

Based on the DP measurements, the permeability of the paste layers coating the aggregate particles in typical pervious concrete is lower than the permeability of conventional concrete. This is plausible since the w/c of the pervious concrete investigated in this study was very low (0.3) in comparison to typical conventional concrete. However, there are insufficient data from the DP test at this time to determine if the test is able to differentiate between a pervious concrete with good durability and a pervious concrete with poor durability.

Future work will involve additional DP test measurements of pervious concrete utilizing different layer thicknesses and water-cement ratio. There are several factors that were not accounted for in the suction modeling. Inclusion of these factors would likely improve the model. Such factors include : Hydraulic action, Tire tread, and Depth of runoff.

REFERENCES

- Agrawal, S. L., Bandyopadhyay, S., Dasgupta, S., and Mukhopadhyay, R. (2008).
“Prediction of dynamic mechanical properties for tire tread compounds,” Rubber
World, (Vol. 237), No. 4, Lippincott & Peto, Inc. Publisher.
- ASTM C 29-97.(1997). “Standard test method for bulk density and voids in aggregate,”
West Conshohocken, PA.
- ASTM C 39-86.(1986). “ Standard test method for compressive strength of cylindrical
concrete specimens,” West Conshohocken, PA.
- ASTM C 78-00. (2000). “Standard test method for flexural strength of concrete (Using
simple beam with third-point loading),” West Conshohocken, PA.
- ASTM C 143-97. (1997). “Standard test method for slump of hydraulic-cement
concrete,” West Conshohocken, PA.
- ACI Committee 522 (2006). “Pervious concrete,” ACI International, Farmington Hills.
- ACPA (2006). “Stormwater management with pervious concrete pavement,”
<<http://www.greenhighways.org>> (Oct.5, 2006).

- Beeldens, A., and Van Gemert, D., Caestecker, C. (2004). "Pervious concrete,"
Laboratory Versus Field Experience, 9th Symposium on Concrete Pavements, Istanbul,
Turkey.
- Carter, C. K. (1975). "Analysis of extreme rainfall events at Austin, Texas, analysis of
extreme rainfall events occurring at Austin, Texas for The City of Austin, Texas : The
comprehensive drainage plan and study," Espey, Houston & Associates, Inc. CIP
Project No. 7029 0.
- Das, B. (1998). "Principles of geotechnical engineering," 3rd edition, Boston, PWS
Publishing Company.
- Descornet, G. (2000). "Low-noise road surface techniques and materials," Proceedings
of Inter Noise 2000, Nice, France, pp. 6.
- El-Dieb, A. S., and Hooton, R. D. (1995). "Water-permeability measurement of high
performance concrete using a high-pressure triaxial cell," Journal of Cement and
Concrete Research, (Vol. 25), No. 6, pp. 1199-1208.
- Francis, A. M. (1965). "Early concrete buildings in Britain," Journal of Concrete and
Constructional Engineering, London, (Vol. 60), No. 2, pp. 73-75.

Fwa, T. F., Tan, S. A., and Guwe, Y. K. (1999). "Laboratory evaluation of clogging potential of porous asphalt mixtures," *Journal of the Transportation Research Board*, No. 1681, pp. 43-49.

Grasley, Z. C. (2006). "Measuring and modeling the time-dependant response of cementitious materials to internal stresses," Ph.D Thesis, University of Illinois at Urbana-Champaign.

Grasley, Z. C., Scherer, G. W., Lange, D.A., and Valenza, J.J. (2006). "Dynamic pressurization method for measruing permeability and modulus : II. Cementitious materials," *Materials and Structures*, (Vol. 40), No. 7, pp.711-721.

Huang, Y. (2004). "Pavement analysis and design," Second Edition, Pearson Education, Inc., Printed in the United States of America.

Kendall, K. (1971) "The adhesion and surface energy of elastic solids," *Journal of Physics, D Applied Physics*, (Vol. 4), No. 8, pp.1188.

Kosmatka, S., Kerkhoff, B., and Panarese, W. (2002). "Design and control of concrete mixtures," 14th Edition, Portland Cement Association, pp. 358.

Kraemer, C. (1990) "Porous asphalt surfacing in Spain," Proceedings of International Symposium on Highway Surfacing.

Kutay, M. E., and Aydilek A. H. (2007). "Dynamic effects on moisture transport in asphalt concrete," Journal of Transportation Engineering, (Vol. 133), No. 7, pp. 406-415. Publisher American Society of Civil Engineers.

Luck, J. D., Workman, S. R., Higgins, S. F, and Coyne, M. S. (2006). "Hydrologic properties of pervious concrete," Transactions of the ASABE, (Vol. 49), No. 6, pp 1807-1813.

Malhotra, V. M. (1976). "No-fines concrete- Its properties an applications," ACI Proceedings Journal, (Vol. 73), No. 11, pp. 628-644.

Marolf, A., Neithalath, N., Sell, E., Wegner, K., Weiss, W.J., and Olek, J. (2004). "Influence of aggregate size and grading on the sound absorption of enhanced porosity concrete," ACI Materials Journal, (Vol. 101), No. 1, pp. 82-91.

Mathis, D. E. (1990). "Permeable bases - An update," PCA, No.8., Nov., pp. 3-4.

Meininger, R. C. (1988). "No-fine pervious concrete for paving," Concrete International, (Vol. 10), pp. 20-27.

Mulligan, A. (2005). "Attainable compressive strength of pervious concrete paving systems," Master Thesis, University of Central Florida.

Nakahara, D., et al. (2004). "Utilization of Pavement Quality Pervious Concrete and its Performance," 9th Symposium on Concrete Pavement, Istanbul, Turkey.

Neithalath, N., Weiss, W. J., and Olek, J. (2003). "Development of quiet and durable porous portland cement concrete paving materials," Final report, The Institute for Safe, Quiet, and Durable Highways, pp. 179.

Nelson, P. M., Philips, S. M. (1994). "Quieter road surfaces," TRL Annual Review, Transportation Research Laboratories, UK, pp. 13.

NRMCA. (2004). "What, why, and how? Pervious concrete," Concrete in Practice Series. CIP 38.

Olek, J., Weiss, W. J., et al. (2003). "Development of quiet and durable porous portland cement concrete paving materials." Final Report, SQDH 2003-5, West Lafayette, IN :Purdue University.

Othman, H. M., Hardiman. (2005). "Characterization of the clogging behaviour of double layer porous asphalt," Eastern Asia Society for Transportation, 6, pp. 968-980.

Park, S., Tia, M. (2004). "An experimental study on the water-purification properties of porous concrete," *Cement and Concrete Research*, (Vol. 34), pp.177-184.

Rogge, D. (2002). "Development of maintenance practices for oregon F-Mix," Final Report, Oregon Department of Transportation Research Group and Federal Highway Administration Washington, D.C.

Sandberg, U. (1999). "Low noise road surface a state of the art review," *Journal of the Acoustical Society of Japan*, Swedish National Road and Transport Research Institute SE-581 95 Linkoping, Sweden.

Sandberg, U. J., Ejsmont, A. (2002). "Tyre/road noise reference book," Informex, Kisa, Sweden, pp. 640.

Schaefer, V., Wang, K., et al. (2006). "Mix design development for pervious concrete in cold weather climates," Final Report, National Concrete Pavement Technology Center, Iowa State University, Ames, IA.

Scherer, G. W. (2006). "Dynamic pressurization method for measuring permeability and modulus : I. theory," *Materials and Structures*, (Vol. 39), pp.1041-1057.

Stoney Creek Materials, L. L. C. Stoneycree-pervious pavement systems.

<<http://www.stoneycreekmaterials.com>> (Feb., 10, 2007).

Tennis, P. D., Leming, M. L., Akers, D. J. (2004). "Pervious Concrete Pavements,"
Special Publication by The Portland Cement Association and the National Ready
Mixed Concrete Association, Skokie, Illinois.

Varadhan, A. (2004). "Evaluation of open-graded and bonded friction course for
florida," Master Thesis of The University of Florida.

Vichit-Vadakan, W., Scherer, G. W. (2002). "Measuring of permeability of rigid
materials by a beam-bending method: III, Cement paste," Journal of the American
Ceramic Society, (Vol. 85), No. 6, pp. 1537–1544.

Yang, Z., Brown, H., Cheny, A. (2006). "Influence of moisture conditions on freeze and
thaw durability of portland cement pervious concrete," Construction and Building
Materials, (Vol. 21), pp. 1034.

Zaldo, M. (2006). "Pervious concrete pavements industry focus," National Ready Mixed
Concrete Association, <www.NRMCA.org> (Oct.5, 2006).

Zouaghi, A., Kumagai, M., Nakazawa, T. (2000). "Fundamental study on some properties of pervious concrete and its applicability to control stormwater run-off," Transactions of The Japan Concrete Institute, (Vol. 22), pp. 43-50.

VITA

Young Min Joung was born in Incheon in Korea. He attended elementary, middle and high school in Incheon. Youngmin obtained his Bachelor of Science degree in civil engineering in Feb. 2006 from University of Incheon. Mr. Joung entered Texas A&M University in September 2006 to pursue his master's degree. Youngmin was employed by the Texas Transportation Institute as a research assistant from September 2006 to September 2007. He was also a research assistant in the Civil Engineering Department. He received his Master of Science degree in civil engineering in December 2008.

His permanent address

101-904 Mujigae heeyoung apartment, Sunhac-Dong, Yunsu-Gu, Incheon, Korea